Doctoral Dissertation

Mechanical Modulation of Inhibitory Pausing State and ATP binding of V_1-ATPase

(1分子操作法によるV_1-ATPaseの反応の角度依存性に関する研究)

Naciye Esma Tirtom

October 2012

Graduate School of Engineering,
Osaka University

工甲 15954

Doctoral Dissertation

Mechanical Modulation of Inhibitory Pausing State and ATP binding of V_1-ATPase

(1 分子操作法による V_1-ATPase の反応の角度依存性に関する研究)

Naciye Esma Tirtom

October 2012

Graduate School of Engineering,
Osaka University

Table of Contents

List of Abbreviations

ATP	adenosine 5'-triphosphate
BSA	bovine serum albumin
DTT	dithiothreitol
PK	pyruvate kinase
LDAO	lauryldimethylamine oxide
LDH	lactate dehydrogenase
NADH	nicotinamide adenine dinucleotide
Ni-NTA	nickel-nitrilotriacetic acid
fps	frame per second
rps	revolutions per second
SP	short pause
LP	long pause

Chapter 1 – Introduction to Rotary Motor, V_oV_1-ATPase

1.1 ATPase Superfamily

1.1.1 V_oV_1-ATPase

Rotary ATPases are a family of enzymes that couple synthesis or hydrolysis of ATP (adenosine triphosphate) with transporting solutes across membrane down or against their electrochemical gradient. One of the member of ATPase family is vacuolar type ATPase, V_oV_1.

V_oV_1 is found in both eukaryotes and prokaryotes (Figure 1.1.1). In eukaryotes this enzyme functions as an ATP-driven proton pump in a wide range of cellular membranes, such as lysosomes, endosomes, secretory vesicles, Golgi-derived vesicles and the plasma membrane of various cell kinds (2,3). Low pH is required to activate the degradative enzymes in the lysosome, therefore transport of small solutes and ions across the lysosome membrane is coupled with ATP hydrolysis. Acidification of endosomes helps the dissociation of receptor-ligand complexes and recycling of unoccupied receptors to plasma membrane. Acidification in endosome is required for budding of endosomal carrier vesicles which move cargo proteins from early to late endosomes. A similar acid-activated dissociation occurs in Golgi-derived vesicles for transporting the lysosomal enzymes from trans-Golgi to lysosome. Plasma membrane embedded V-ATPases in renal intercalated cells secrete protons into urine, having a role in regulation of plasma pH. In osteoclasts this enzyme transports protons to degrade the bone. V-ATPase is also found in the plasma membrane of macrophages and neutrophils, participating in regulation of pH homeostasis. In epididymus and vas deferens, it serves for sperm maturation and storage.

In prokaryotes, this enzyme is found in plasma membrane of some eubacteria, such as *Enterecoccus hirae*, *Thermus thermophilus* and archaea (Figure 1.1.1). These are sometimes classified as another member of ATPase family, archaeal -type ATPase (A-ATPase) or A_oA_1; though we prefer to refer them as prokaryotic V-type ATPases (4).

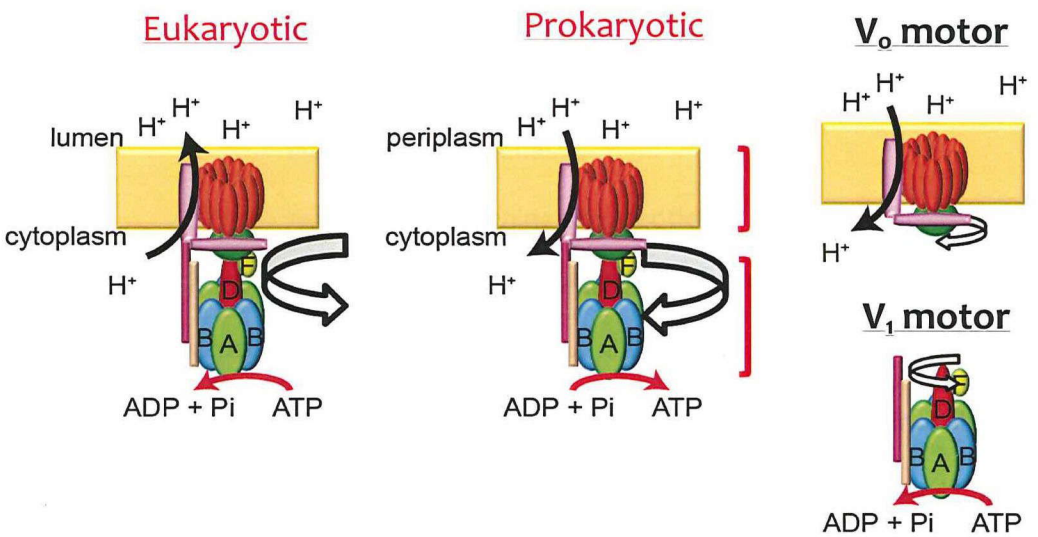

Figure 1. Structure of V_oV_1-ATPase from eukaryotes (left) and prokaryotes (right). Eukaryotic V_oV_1-ATPase has additional subunits which are not shown here. In eukaryotes, V_oV_1-ATPase functions as a proton pump by hydrolyzing ATP, and in archaea and some of eubacteria, it functions as ATP synthase with pumping protons along the electrochemical potential.

In archaea and *Thermus thermophilus*, this enzyme functions as an ATP synthase while transporting protons through the membrane down their electrochemical potential (5). For coupling these two functions, this enzyme is composed of two distinct motor domains; hydrophilic, cytoplasmic portion V_1, which catalyzes ATP synthesis and hydrophobic, membrane-embedded V_o, which transports ions through the membrane. These domains are coupled via the rotation of a central stalk against the surrounding stator complex.

V_o motor generates the rotary torque upon proton translocation driven by electrochemical potential through the membrane. And V_1 part, in response to rotary torque from V_o motor, synthesizes ATP (Figure 1).

V_1 motor consists of 4 different subunits with a stoichiometry of A3B3DF (6). A3B3 makes up the hexameric ring, where A and B subunits are alternately arranged. D and F subunits make up the central rotary shaft, and fills in the cavity of A3B3 ring.

V_o motor is composed of L ring, C, I subunits and EG peripheral stalks (7,8). L ring in *Thermus thermophilus* is composed of 12 subunits. On top of the ring there is the C subunit interacting with DF rotary shaft of V_1 motor. L ring rotates against the membrane-embedded portion of I subunit, in the opposite direction of DF shaft rotation in V_1. So, in the whole complex, V_1 and V_o push each other in opposite direction.

When V_1 motor is isolated from the hydrophobic V_o motor, it acts as an independent motor, rotating the central shaft for hydrolyzing ATP into ADP (adenosine diphosphate) and Pi (inorganic phosphate) (6). Due to its function, it is called as V_1-ATPase.

1.1.2 F_oF_1-ATPase

Another member of ATPase family is famous F_oF_1-ATPase. F_oF_1-ATPase is found in mitochondrial inner membrane, thylakoid membranes and bacterial plasma membrane (Figure 2). F_oF_1-ATPase catalyzes ATP synthesis coupled with transmembrane proton flow (9). When there is enough electrochemical potential of the protons in the membrane, then this enzyme synthesizes ATP from ADP and Pi. It converts the electrochemical potential into its chemical form in ATP (10). But when the electrochemical potential is insufficient, then

this enzyme works in reverse direction to generate electrochemical potential across the membrane by catalyzing the pumping of protons with hydrolysis of ATP into ADP and Pi.

This enzyme, similar to V_oV_1-ATPase, is composed of two motor domains, water-soluble part F_1-ATPase and memrane-embedded F_o motor.

Bacterial F_1 motor is composed of five different subunits with a stoichiometry of $\alpha 3\beta 3\gamma\delta\varepsilon$. Alternately arranged 3 α and 3 β subunits make up the hexameric stator ring. γ subunit, rotor shaft, fits into the central cavity of $\alpha 3\beta 3$ ring. ε subunit binds to the protruding portion of γ shaft, and makes a connection between rotor parts of F_1 and F_o domains. ε subunit is the endogenous inhbitor of F_1, by blocking the rotation of γ due to steric hindrance via changing its conformation from closed to extended structure (11). δ subunit acts a connection between stator parts of F_1 and F_o. The minimum ATPase active F_1 complex is $\alpha 3\beta 3\gamma$.

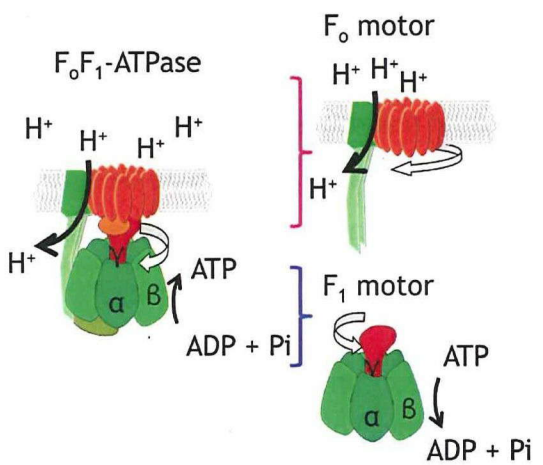

Figure 2. Schematic drawing of structure of F_oF_1-ATPase. Similar to V_oV_1-ATPase, F_oF_1-ATPase is also composed of two domains, membrane-embedded F_o motor and cytoplasmic part F_1 motor.

F_o motor consists of ab_2c_{10-15}. The number of c subunits varies among species. In *E. coli* it is 12 (12), and in *Bacillus PS3* it is 13 (13). c subunits make up the ring structure, cavity of which is filled by γ shaft. c ring rotates against ab2 stator complex.

Similar to V_1, F_1 also acts as an ATP-driven rotary motor, when isolated from the membrane portion F_o. Free F_1 motor rotates γ shaft to hydrolyze ATP.

1.2 Rotary Catalytic Mechanism of V_1 and F_1

1.2.1 Rotation of V_1 – so far revealed

V_1-ATPase, when isolated from the whole complex, catalyzes ATP hydrolysis while rotating the central shaft. So far, V_1 has been studied both in biochemical and single-molecule experiments (Figure 3). In 1998, a biochemical experiment (5) showed that after several min of hydrolyzing ATP, all the V_1 molecules lost their activities (Figure 4). Moreover when V_1 molecules were pre-incubated with ADP, losing the activity was hurried. In the same study, ATP binding of isolated subunits were determined: B subunit did not bind ATP, however A subunit showed a strong affinity for ATP. So, the catalytic reaction center resides at the A-B interface, mainly on A subunit (5).

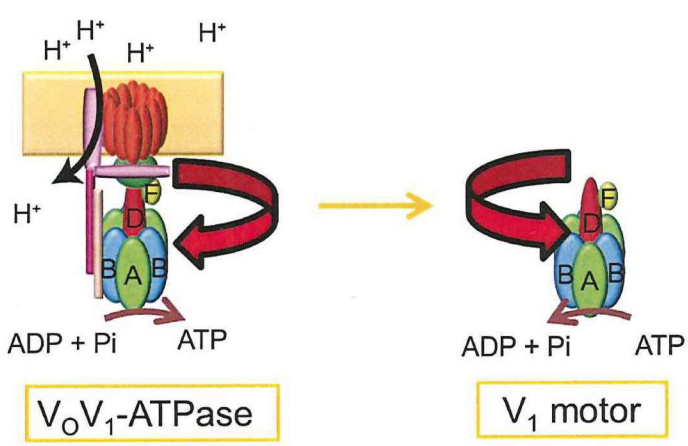

Figure 3. V_1-ATPase, when separated from the whole complex, acts as an independent motor: Though its physiological role is to synthesize ATP, when isolated, it hydrolyzes ATP.

The direct observation of rotation of V_1 was achieved on 2003 by Dr. Imamura (14). To visualize the rotation of the shaft, a probe was attached to D or F subunits of central shaft, where the stator A3B3 ring was immobilized on glass by 10xHis tags (Figure 4). It was shown that central shaft rotates in counterclockwise direction when viewed from membrane side. In a later single-molecule study (15), V_1 was observed to rotate in 3 step behavior, where each step (120°) was taken with hydrolysis of a single ATP molecule. Torque for rotating one step was calculated from the angular velocity of the bead and the frictional load (bead) (16). Torque of V_1 due to hydrolysis of one single ATP molecule was 35 pN·nm (Figure 6). In the same study, by using a slowly hydrolyzable ATP analogue, authors showed that ATP hydrolysis takes place at the same angle with ATP binding (Figure 5).

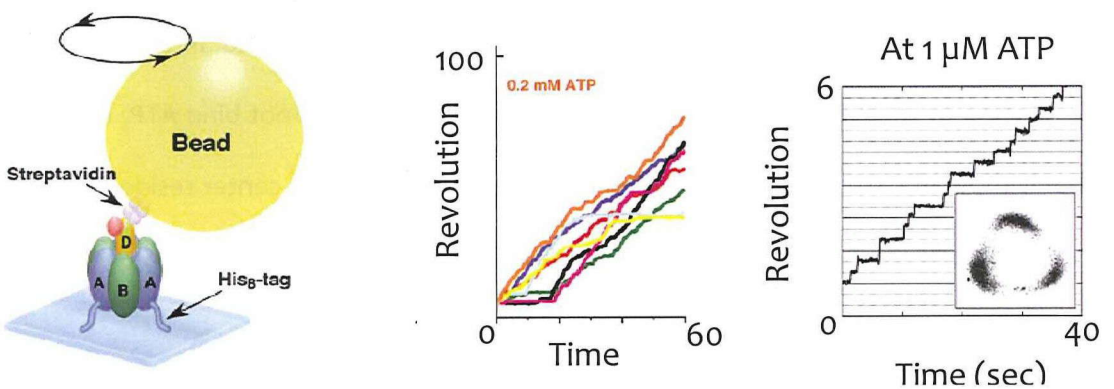

Figure 4. *A*, Rotation of V_1-APase was first observed in 2003 by using this experimental setup (14). The probe used for as a rotation marker was attached to D or F subunit. *B*, Graph shows the trajectories of several rotating molecules at 0.2 mM ATP. *C*, 3-step rotation of V_1-ATPase was observed under non-saturating [ATP] (14).

A recent study confirmed binding and hydrolysis events occur at the same position, by observing the rotation with a drag-free 40 nm gold colloid as a probe, under high-speed camera (17). The authors concluded the dwell time between each step at saturating [ATP] is around 5 ms, sum of two events' dwell. One event was defined as ATP hydrolysis and the other could be release of one of the products (ADP or Pi), or both of them.

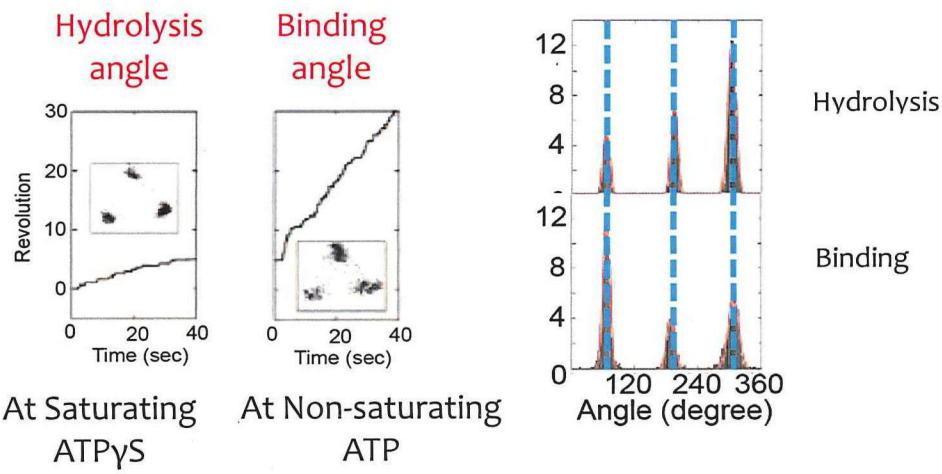

Figure 5. Angular position for ATP hydrolysis and binding were compared, by performing a buffer-exchange experiment (15). First rotation was observed under saturating ATPγS concentration, which is a slowly-hydorlyzable analogue of ATP. After assigning the angular positions for ATP hydrolysis, buffer was exchanged to non-saturating ATP concentration, where ATP-binding reaction becomes rate limiting step.

1.2.2 Rotation of F_1

F_1-ATPase is, so far, the best-studied ATPase. And the studies done on F_1-ATPase paved the way for other ATPases, like V_1-ATPase.

The first crystal structure of F_1 was revealed in 1994 (18). The famous 'binding-change mechanism' model was suggested based on this structure: Three β subunits work

cooperatively, where each subunit sequentially shifts from closed to open conformation. (19). Based on this structure, the unidirectional rotation of γ in F_1 was hypothesized.

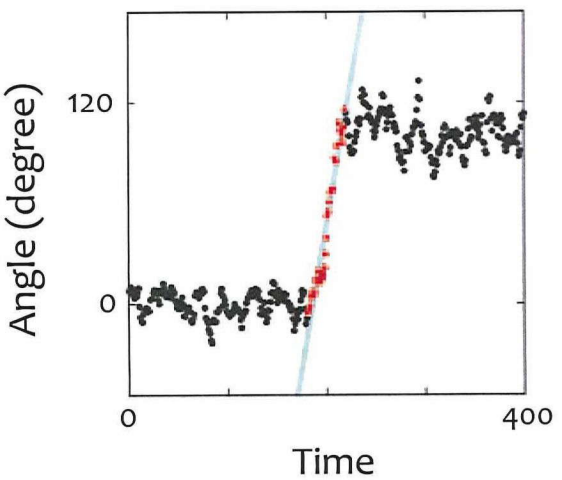

Figure 6. Torque generated by hyrolysis of a single ATP molecule was calculated from the stepping angular velocity and frictional coefficient of the bead (15).

After this study, many researchers tried to show the rotation of F_1. The direct observation of rotation of F_1 (thermophilic *Bacillus PS3*) under microscope was achieved in 1997 (20). A single F_1 protein was fixed onto glass from the N termini of beta subunits. The γ subunit was attached a fluorescently-labelled actin filament (several μm length), to magnify the rotation orbit which was in 2 nm diameter. The rotation was always in counterclockwise direction when viewed from F_o motor or membrane side. The rotation was too slow due to huge viscous load, but this helped to determine the torque from one single step (120°). Torque was calculated as 40 pN·nm.

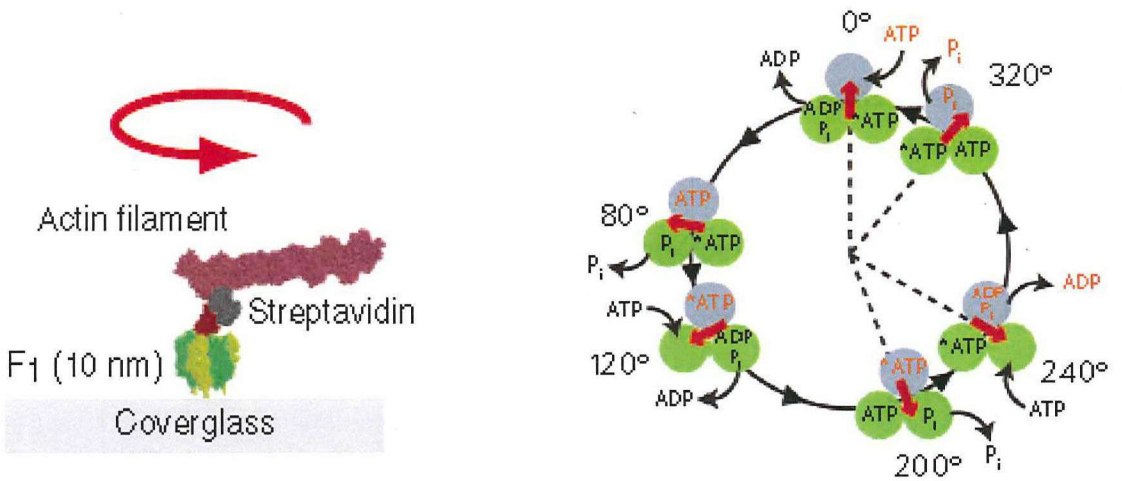

Figure 7. *A*, Rotation of F_1-ATPase was first observed by attaching an actin filament to rotary shaft (20). *B*, In this scheme, a single turn of shaft was shown. Circles and red arrows represent the catalytic states of beta subunits and angular positions of gamma subunit (21). The hydrolysis of a single ATP molecule which binds to top beta subunit occurs as follows: ATP binding at 0° ; hydrolysis, 200° ; ADP release 240° and Pi release 320° .

Later on, 3-step rotation consistent with the presence of 3 catalytic sites were observed, when ATP was supplied under K_m (1 μM). The mean dwell between steps corresponded to binding of a single ATP molecule (22). To observe the hydrolysis dwell, a much smaller probe (40 nm gold colloid) was used. Under K_m, two substeps of 80° and 40° were detected to occur in a single 120° step (23,24). Dwells at 0° and 80° occurs due to binding and hydrolysis reactions, respectively. Further single molecule studies revealed the scheme of rotation and single ATP catalysis as follows: ATP binding, 0° ; hydrolysis, 200° ; ADP release, 240° and Pi release 320° (23,25-29).

In 2001, a single molecule study showed that F_1 molecules lapse into 30-sec scale pause, which corresponds to ADP-inhibited state of F_1 (30). F_1 molecule shows this inhibitory pausing state because it could not release its reaction product, ADP-Mg (31).

1.3 Mechanochemical Coupling in V_1

V_1-ATPase and also F_1-ATPase works as ATPase when isolated from the whole complex. However, in some species, physiological function of these motors is to synthesize ATP, not to hydrolyze. For example, *T.thermophilus* has V_oV_1-ATPase for synthesizing ATP (6), even though *E. hirae* has it for proton pump (32).

An impressing feature is the switching of function in V_1-ATPase (or in F_1) in parallel with the direction of rotation. Let's consider the case of *T. thermophilus* V_oV_1-ATPase (Figure 8). In the whole complex, shaft is rotated in clockwise direction due to enforcement by V_o motor, though it is reversed in the case of isolated V_1-ATPase. When V_1 motor synthesizes ATP, shaft rotates clockwise; and when it hydrolyzes ATP, shaft rotates counterclockwise. This relationship between the mechanical rotation and chemical reaction is called as mechanochemical coupling (25).

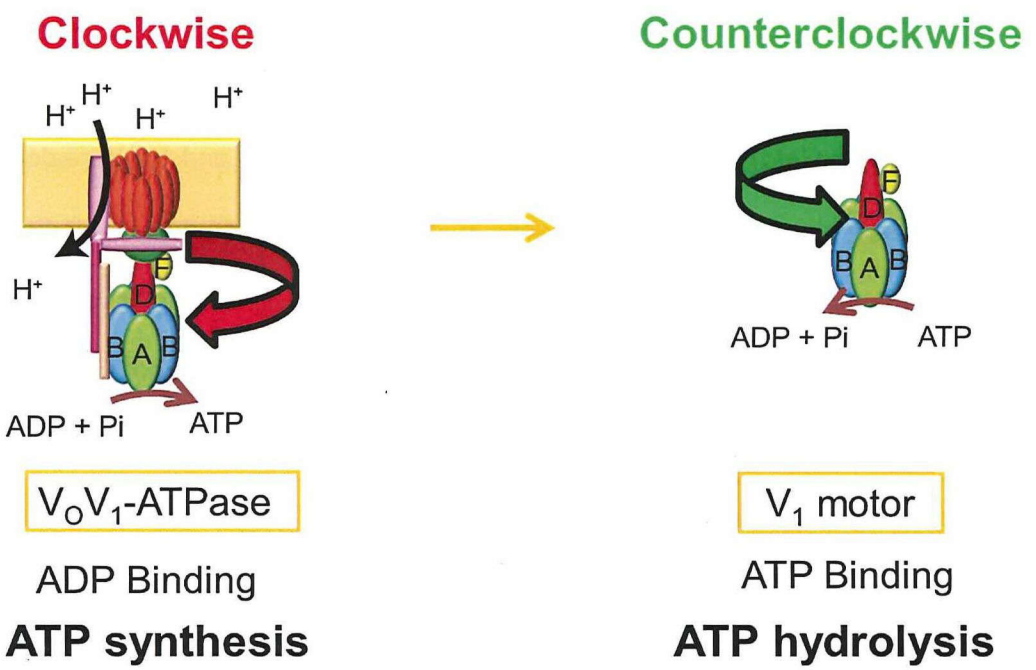

Figure 8. Mechanochemical coupling scheme of V_oV_1-ATPase. Rotation direction of the shaft is related with the chemical reaction being held. When the shaft rotates clockwise obeying the V_o domain, V_1 motor synthesizes ATP. However, when V_1 motor is separated from the whole complex, it just hydrolyzes ATP while the shaft is rotating in counterclockwise direction.

This reversibility in mechanochemical coupling implies that chemical reactions are regulated by rotation of shaft (Figure 9). The chemical equilibirum in each individual reaction of ATP hydrolysis (ATP binding, hydrolysis and product release) should be modulated by shaft's rotation in V_1-ATPase. So, exploring the kinetics of transient conformational states achieved during shaft's rotation could enlighten us about the mechanochemical coupling mechanism in V_1.

So far, several studies were performed for understanding the reversibility of mechanochemical coupling mechanism in F_1 (21,29,33), which will be covered in following chapters as a means of comparison with data of V_1-ATPase.

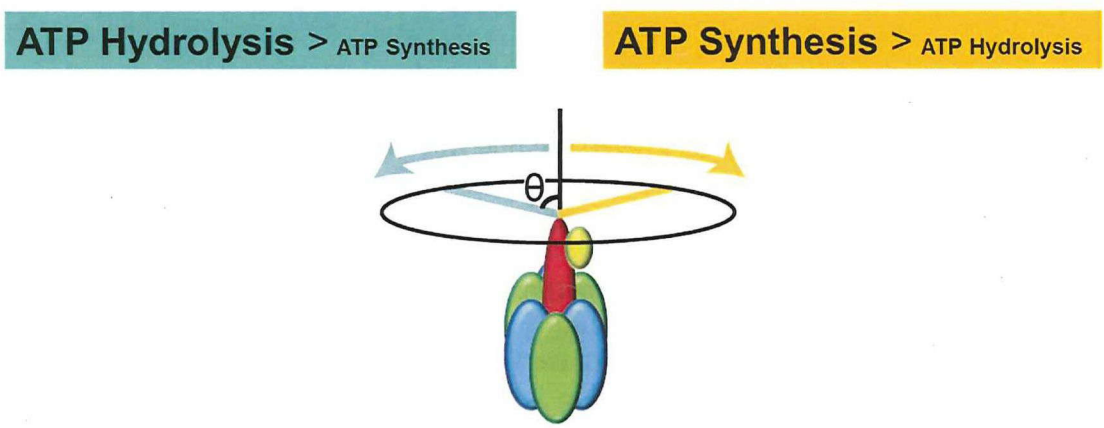

Figure 9. Chemical reactions are regulated by rotary angle of the shaft. The equilibirum between ATP hydrolysis and synthesis is balanced via the rotation direction of the shaft.

When the shaft rotates in clockwise direction, ATP synthesis is favored over hydrolysis; and when it rotates counterclockwise, the opposite happens.

1.3 Objective of this study

This study aimed to uncover the mechanochemical coupling mechanism in V_1-ATPase. As stated in previous section, the reversibility of mechanochemical coupling is an important feature of both V_1 and F_1-ATPase. Even though several studies was performed for F_1-ATPase, V_1-ATPase still awaits being analyzed. One way to study this coupling mechanism passes through the understanding of the kinetics and chemical equilibrium of individual reaction steps of ATP hydrolysis. With this purpose in mind, I started to analyze the kinetics and equilibrium of ATP binding event by using a mechanical manipulation method, which is explained in next section, 'Experimental Techniques'.

However, during attempts of mechanical manipulation of ATP binding event, V_1 molecules were observed to frequently lapse into some pauses and after a while to stop rotation completely. To prevent the interference of these pauses to our analysis of ATP binding event, we decided to characterize these two pauses first. The results related to these pauses were explained in Chapter 2. The frequently observed second-scale pause was named as short pause. And the final, irreversible one was called as long pause. The angular positions and the kinetics of these pauses were determined. Finally, the long pause state was mechanically manipulated to check whether the molecule can resume rotation. This technique was proved to be successful because V_1 molecules in long pause state resumed rotation upon our manipulation. The suppressing effect of ADP on exit from long pause implied that long pause represents the ADP-inhibited state of V_1-ATPase.

After characterization of pausing behavior of V_1-ATPase, mechanical manipulation of ATP binding event was studied. Results for this part of my study were covered in Chapter 3. Manipulation was performed at non-saturating ATP concentrations, where clear ATP-waiting dwells were observed. ATP binding rate increased when the molecule was manipulated in the direction of rotation. The torque generated by ATP binding event was calculated from the slope of rotary potential of ATP-bound state. The contribution of torque by ATP binding is less signicant in V_1 compared with F_1.

In the final chapter, the future works which should be following this study were discussed. Mechanical manipulation of other reaction steps should be performed to complete the whole puzzle of mechanochemical coupling mechanism.

1.4 Experimental techniques

The following methods were used for single molecule observation and manipulation, results of which were covered in Chapter 2 and 3.

1.4.1 Wild type V_1 vs TSSA mutant V_1

During my PhD study, I used V_1-ATPase from *Thermus thermophilus*. This bacteria does not have F_oF_1-ATPase, instead it has large amount of V_oV_1-ATPase located on its plasma membrane (34).

Single molecule biophysicists, who worked with *T. thermophilus* V_1-ATPase, used either wild type or TSSA mutant of this protein. In 2003, direct observation of the rotation of V_1-ATPase was shown using TSSA mutant (14).

Wild type V_1-ATPase has strong tendency to lapse into ADP-inhibited state during catalytic turnovers (31). V_1 molecules stopped rotation within ≈5 min after addition of ATP (14). This led scientists to search for mutations which can prevent or postpone ADP inhibition. A double substitution (S232A/T235S) in A subunit suppressed ADP inhibition to allow observation of rotation around 1 hr after introducing ATP. So far, most of the single molecule works focused on TSSA mutant of V_1-ATPase (14,15,35-37), though there are also works done with wild type V_1-ATPase (17,36,38).

In my PhD course, I preferred to use wild type V_1-ATPase due to that our final goal is to understand the working mechanism of V_oV_1-ATPase under physiological conditions. We would like to compare the characteristics of wild type V_1 with that of wild type F_1 to have a better understanding about general features of ATPase superfamily.

1.4.2 Rotation assay

Coverslips coated with Ni-NTA were prepared as described in Appendix section. A flow cell of 5–10 µl in volume was made of two coverslips (bottom, 24 × 36 mm^2 and top, 24 × 24 mm^2) separated by two spacers of 50-µm thickness. Biotinylated V_1–ATPase in buffer A (50 mM Tris-HCl (pH 8.0), 100 mM KCl) was infused into a flow cell and incubated for 5 min. V_1-ATPase had tags of 10 Histidine residues attached to the N-terminus of A subunits. These His tags interacted with Ni-NTA moieties on the surface of bottom coverslip (top coverslip was not coated with Ni-NTA). Unbound V_1 was washed out with 50 µl of buffer A.

Then buffer A containing 1% BSA was infused into the flow cell to reduce nonspecific binding of the beads or colloid particles. After incubation for several minutes, the solution of a rotation marker particle, magnetic beads (Seradyn, Thermo Scientific, USA), or the custom

colloidal gold beads was infused into the flow cell. After incubation for 20 min or more, unbound beads were washed out with 70 µl buffer A. Observation of rotation was initiated after infusion of 140 µl buffer B (50 mM Tris-HCl pH 8.0, 100 mM KCl, 2 mM $MgCl_2$) containing an indicated amount of Mg-ATP.

For ADP-free experiments, ATP regenerating system (50 µg ml pyruvate kinase, 1 mM phosphoenol pyruvate) was added to buffer B. Rotation of the bead was observed under phase-contrast microscopy (IX70, Olympus) using a 100× objective lens (Figure 10). Images were captured with a charge-coupled device camera (FC300M; Takenaka) at 30 frames per sec (fps). Analysis of rotation was performed using custom software (Digimo). Time-averaged rotation speed was calculated over 5 consecutive revolutions. All experiments were carried out at 23–25°C.

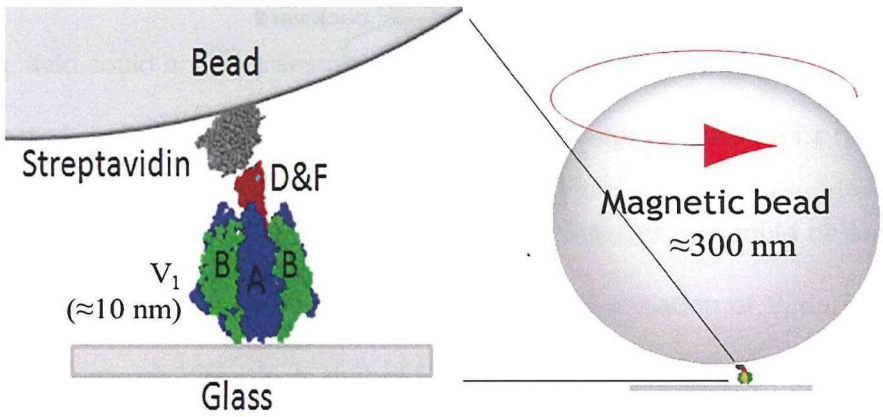

Figure 10. Side view of the experimental setup for observing rotation. The size of V_1-ATPase is around 10 nm, though the diameter of magnetic bead we used is app. 300 nm. Because of the huge viscous load, rotation of V_1 was impeded; rotation rate drastically decreased. For one experiment, we also used 40 nm colloidal gold as a rotation marker to reduce the viscous friction caused by the load.

1.4.3 Mechanical manipulation with magnetic tweezers

A simplified diagram for magnetic tweezers is shown in Figure 11. Detailed explanation can be found in Appendix section. Tweezers is composed of 2 pairs of crossed electromagnets, which is made of an iron core (10, 10, 40 mm) and a copper wire which surrounds the core for 100 turns. The electromagnets in one pair are separated by 15 mm, and this setup is placed 10 mm above the microscope stage. The electromagnets are connected with electricity in series. The microscope stage and magnetic tweezers are made of antimagnetic materials. The magnetic field is generated as explained: One pair (y axis) of electromagnets is applied current of having sine components, and the other (x axis) is current of having cosine components. Magnetic field strength can be changed by current amplitude.

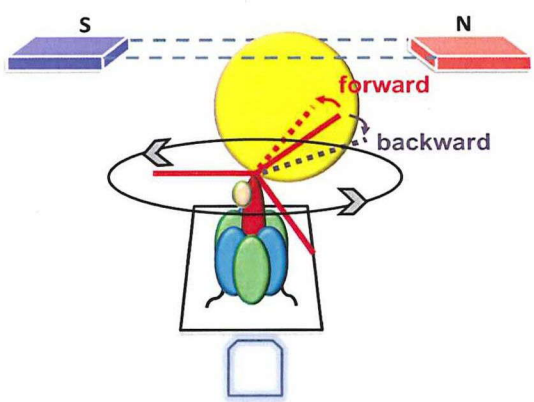

Figure 11. Magnetic tweezers setup for mechanical manipulation of the rotary shaft. With this setup, we can stall the bead at a desired angle or rotate it in desired direction.

With this magnetic tweezers setup, we could manipulate the shaft's rotation via the attached magnetic bead. With the custom software, we could input the desired magnetic field's direction and the time period for manipulation. For instance, we can rotate the bead to a certain angle, and make it stay there for certain time and then cut the magnetic field. In

this case to reach the desired angle takes around 0.1 sec, from the original angle. Or we can rotate the bead for several revolutions where the speed of forcible rotation could be user-input. In both studies covered in Chapter 2 and 3, the prior example of manipulation was employed for studying the response of transient conformational states regarding the chemical reaction of interest. This results obtained by using this manipulation technique will be covered in more detail in the related sections of the Chapter 2 and 3.

Magnetic moment of some magnetic beads was not parallel to the microscope stage, therefore when magnetic field was applied, they were inclined. These molecules were not analyzed.

Whether the angle of rotary shaft is same as the angle of magnetic bead is not clear. There are some studies performed for calculating the stiffness of the setup for F_1 motor (39). It was shown that system has some elastic components, implying that the effect of applied magnetic field could not be transmitted to the shaft in the same magnitude (39-41). For F_1, the corrected angle of the shaft deviated from that of magnetic bead in 1:4 ratio.

The angle values for V_1 also need to be corrected. However, we could be sure about the transmission of magnetic field effect, because rotary fluctuation of V_1 during the pausing state does not greatly differ from that of F_1-ATPase (15), implying that rigidity of the shaft in both proteins should be somehow similar.

Chapter 2. Two pauses of V_1-ATPase and mechanical modulation of long pause state

Main objective during my PhD study was to mechanically manipulate the individual reaction steps during ATP hydrolysis (Figure 12). However, we observed that V_1-ATPase shows some pauses during rotation and after a while stops rotation completely. Therefore, as a first step, we decided to analyze these pausing states of V_1 for determining the interference from these pauses in the individual reaction steps. Then we could continue with our main objective of mechanical manipulation of individual reaction steps.

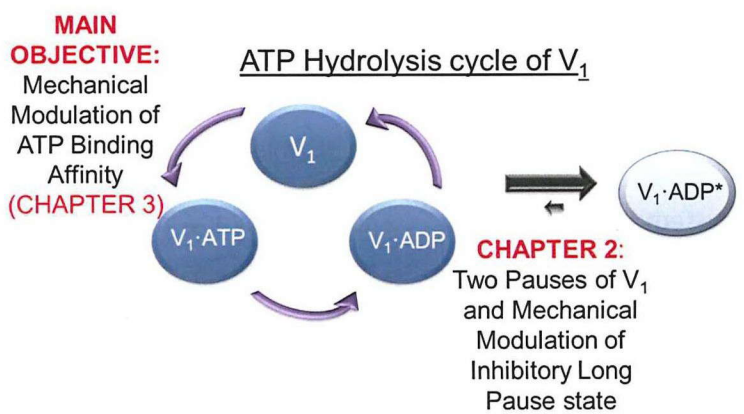

Figure 12. My main objective during PhD study was to mechanically manipulate the ATP binding reaction for a better understanding of mechanochemical coupling mechanism of V_1. However during rotation assay we observed that V_1-ATPase lapses into some inhibitory pausing states. Before continuing with the real objective, we decided to analyze these pauses.

2.1 Inhibitory Pauses during rotation of V_1

Rotation of V_1 was observed at single-molecule level by attaching a magnetic bead of 200-500 nm in diameter as a probe to D subunit of the rotary shaft (Figure 13) (38). A3B3 ring

was immobilized on glass surface through the His-tags introduced at A subunits. Rotary motion of the V_1 motor was visualized as the rotation of the magnetic bead, under phase-contrast microscope.

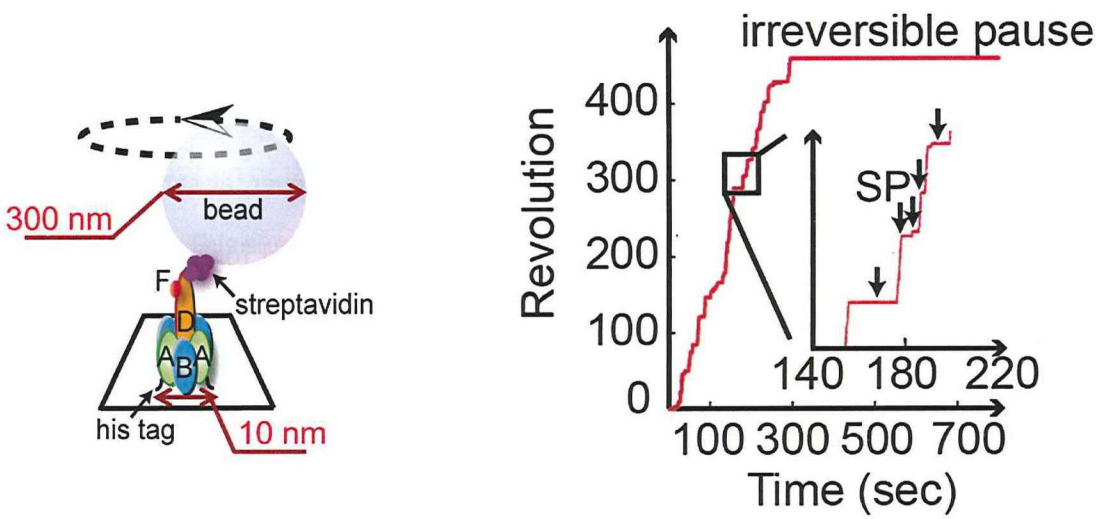

Figure 13. Rotation assay scheme (not to scale) with magnetic bead (38). Rotation trajectory of a single rotating molecule where both reversible short pauses and irreversible long pause were displayed. Short pauses are second-scale transient pauses that were frequently encountered during rotation. After several min of rotation, every molecule entered into an irreversible pause which we named as long pause, to distinguish it from short pause.

First we drew the Michaelis-Menten curve of the V_1 motor with attached probe of magnetic bead (Figure 14). Previous literature showed Michaelis-Menten curves of TSSA V_1 with duplex polystyrene beads of 220 (36) and 340 nm (15) diameter, and of WT V_1 with gold colloid of 40 nm diameter (17). Due to high viscous friction against the big magnetic bead, rotation rate was limited to approximately 8 rps. Rotational velocity was determined at varying ATP concentrations from 0.5 μM to 4 mM. Vmax and Km were determined to be 3.8 rps and 8.1 μM, giving the apparent rate constant of ATP binding as 1.39×10^6 $M^{-1}s^{-1}$, which

was consistent with k_{on}^{ATP} values obtained from using 40 nm gold colloid (17) and ATP hydrolysis activity (36).

A typical time course of V_1 rotation at 4 mM ATP (saturating) can be seen in Figure 13. Time constants of ATP-binding dwell and ATP-cleavage dwell are 0.3 ms and 2.5 ms (17), respectively, which are negligible as compared to time for a single 120° rotation (~42 ms). Therefore, V_1 molecules generally followed smooth rotation. However, at saturating [ATP] such as 4 mM, rotation of the molecule was frequently interrupted for several seconds, which is too long to be related with ATP binding or catalytic dwell of 0.3-2.5 ms. These pauses were transient, so V_1 molecules spontaneously resumed rotation with the completion of pause.

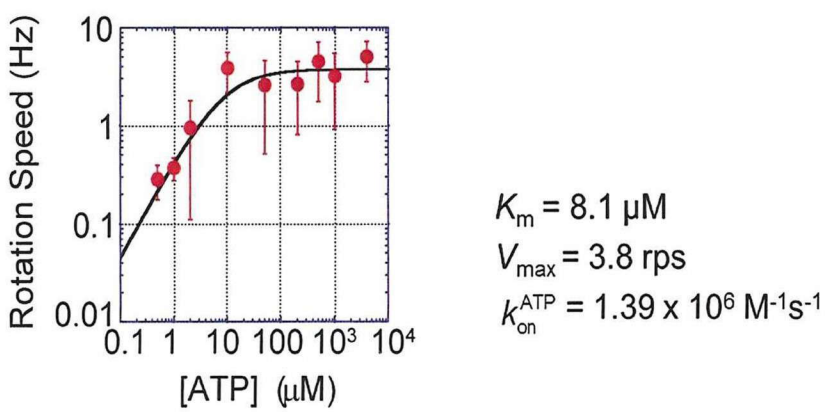

Figure 14. Michaelis-Menten curve of V_1-ATPase based on rotation assay with magnetic bead (38). Due to high-viscous load, V_{max} was found to be 3.8 rps, and k_{on}^{ATP} was calculated as 1.39 x 10^6 $M^{-1}s^{-1}$. V_{max} obtained from rotation assay with 40 nm gold colloid was 64 rps, almost same as that obtained from viscous-free ATPase assay.

These transient pauses always occurred in one of 3 angular positions separated by 120°, which are consistent with the pseudo-3-fold symmetrical structure of V_1-ATPase. This suggests that the pause was due to a slow transition to a catalytically inactive state. This

'rotate – pause – rotate' type of activity was observed until the V_1 molecule completely stopped.

The V_1 molecules never reactivated from this final pause, even if several hours passed. At maximum 6 hours was waited to observe if there will be any spontaneous reactivation; however, molecules didn't resume rotation. So, this final pause was practically irreversible. The angular position of this final pause always coincided with one of the 3 angular positions of short pause. This suggests that final pause is also caused due to an intrinsic inactivation process.

From now on, for simplicity, we will call the final, irreversible pause as long pause (LP), and second-scale, reversible pause as short pause (SP).

2.2 Angular position of the pauses

For characterization of SP and LP states, we first wanted to determine the angular positions of SP and LP in relation to the ATP-waiting angle. For this purpose, we carried out a buffer-exchange experiment during rotation assay.

First, rotation was observed under ATP-limiting conditions to determine the ATP-waiting angles for individual molecules. At 4 μM ATP, which is well below the K_m, 8.1 μM, the overall reaction rate is determined by the ATP binding step, and V_1 mostly spends time in an ATP-waiting pause.

Before continuing with the buffer exchange experiment, I want to clarify one important issue at ATP-limiting conditions: Does short pause occur even at non-saturating ATP concentrations?

We noticed the presence of short pause state, for the first time under ATP-saturating conditions (4 mM). However, if short pause was observed even under at non-saturating

ATP concentrations, then we cannot say that the rate-limiting reaction at [ATP] below K_m, is ATP-waiting pause. To check this point, we determined the dwell time of all transient pauses including both ATP-waiting pause and short pause, at several ATP concentrations. The transient pause even as short as 1 frame, 0.033 sec, was counted. Figure 15 shows the dwell time histograms of transient pauses, under [ATP] from 0.05 μM till 4 mM. The time constants derived from the single exponential fitting of the histograms were plotted against corresponding [ATP]. The time constants including 10 μM ATP showed clear dependence on [ATP], though above 10 μM ATP was almost constant around 4 sec (Figure 16). The values until 10 μM, close to K_m, were consistent with theoretical time constants calculated by using k_{on}^{ATP}. This implies the occurrence of short pause was much lower than that of the ATP-waiting pause at non-saturating [ATP]. However, we could not precisely indicate the occurrence frequency of short pause at non-saturating [ATP]. Based on this dwell time analysis, we concluded that the pauses observed at 4 μM ATP mainly occur due to waiting for ATP.

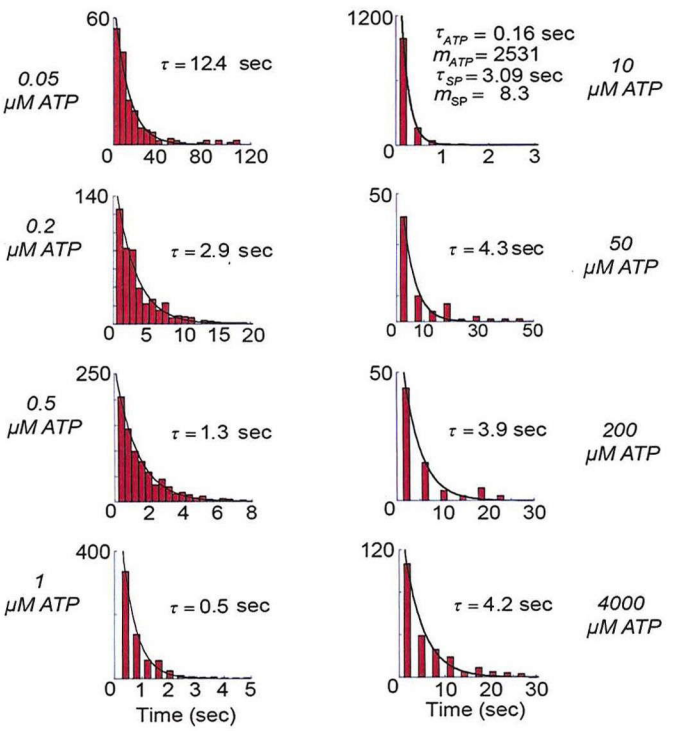

Figure 15. Dwell time analysis of transient pauses at varying ATP concentrations that are displayed on the side of graphs (38). Except 10 μM ATP, all conditions were fitted with single exponential. Data from 10 μM ATP ($\approx K_m$) was fitted with double exponential, which gave two time constants, representing ATP binding dwell and short pause. Until K_m, time constants simply showed [ATP] dependence. Though above K_m, time constants were almost same around 4 sec.

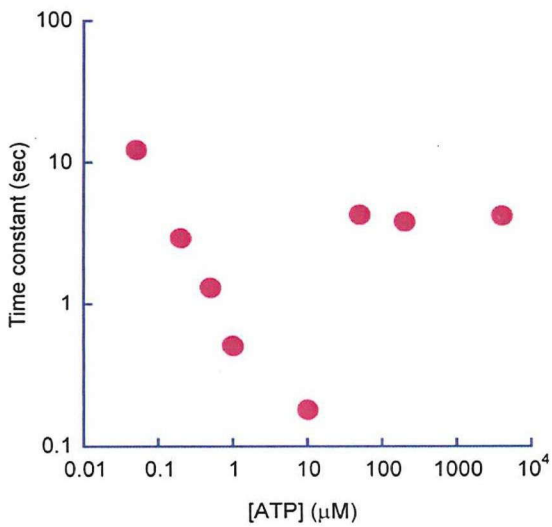

Figure 16. ATP dependence of transient pauses, including both short pause and ATP-waiting pause (38). After $K_m \approx 10$ μM, time constants remained constant around 4 sec, implying that effect of short pause at non-saturating [ATP] is negligible. However, it becomes significant at high [ATP].

So, ATP-waiting angles (Figure 17A) were simply determined as three peaks found in the histogram of the angular position during the rotation (Figure 17B, top) (38). After we found the molecules that showed 3-fold symmetry pausing equally at three ATP-waiting angles, the buffer was exchanged with buffer containing 4 mM ATP, where the ATP-waiting pause diminished and short pause became prominent. Angular histogram during rotation at 4 mM showed the three positions of short pause (Figure 17B, below). It is quite clear that angular

positions of *SP* coincided well with those of the ATP-waiting angles. The angular difference of *SP* from the ATP-waiting angle was only 0.6 ± 12° (mean ± SD; *n* = 48) (Figure 17C). Thus, we can conclude that short pause share the same angular positions with ATP-waiting angles. Later, we wanted to determine the angular position of long pause. For this, we simply monitored the molecules' rotations until lapsing into long pause, at saturating [ATP], 4 mM (38). Until final LP state, the molecules show frequent short pauses. And we are already clear about the short pause's angular position relative to ATP-waiting angle. Therefore we could determine the angular position of LP by comparing with short pauses' angular positions. As shown in Figure 18*A* and *B*, the angular position of *LP* was approximately identical to one of the three angles of *SP*. The angular deviation determined from statistical analysis (Figure 18C) was −0.1 ± 7.2° (mean ± SD; n = 29). Thus, *LP* also shares the same angular position with ATP-waiting angle.

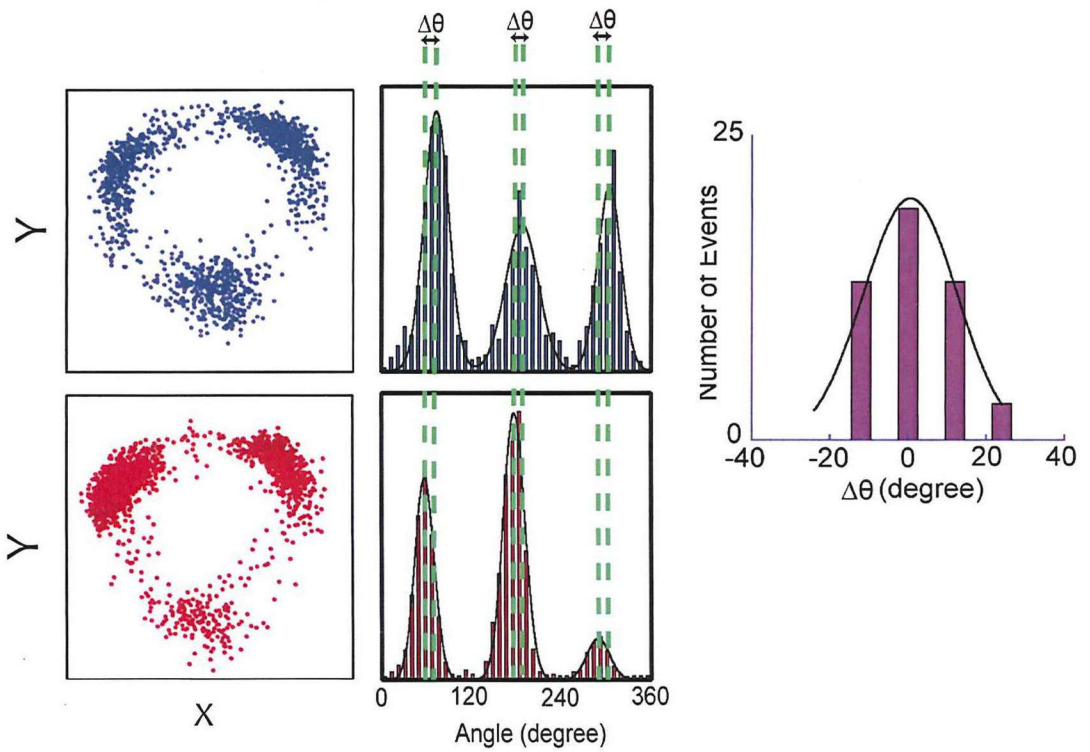

Figure 17. Short pause and ATP-waiting pause share the same angular position (38). By performing a buffer-exchange experiment, we determined the angular positions for both kinds of pauses. First rotation of a single molecule was observed at non-saturating ATP concentration, where ATP-binding is rate-limiting step. Then buffer of chamber was exchanged to saturating ATP concentration, where short pause becomes significant. ATP-binding event cannot be observed at saturating [ATP] due to very small time constant and low time resolution of camera.

2.3 Kinetic Analysis of Pauses

Next we wanted to determine the kinetic parameters of short and long pauses. Regarding the short pause, Figure 19 shows the histograms of the duration time of short pause and rotation time between two successive short pauses, respectively. The histograms were fitted with single exponential decay, providing time constants of the inactivation into short pause and activation from short pause, $\tau^{SP}_{Inactivation}$ (0.9 s) and $\tau^{SP}_{Activation}$ (4.2 s), respectively. Thus, V_1 remained in the active state (rotation state) for only 18% of the observation time. The free energy difference of the inactive state (*SP* state) from the active state (rotation state) was estimated from the equilibrium constant (0.21) of the active state to be -1.5 k_BT, where k_BT represents the thermal energy.

Biochemical studies have reported that *T. thermophilus* V_1 lapses into the ADP-inhibited form during ATP hydrolysis (14), the time constant of the inactivation in the literature (~3 min) is too long to reflect *SP* (5). However, the literature value is rather close to the rotation time until lapsing into *LP*.

Figure 20 shows the histogram of the rotation time before *LP* including both the rotation time and the duration time of *SP*. Fitting of the histogram with single exponential decay gave the time constant of inactivation into LP state, $\tau^{LP}_{Inactivation}$, of 17.6 min.

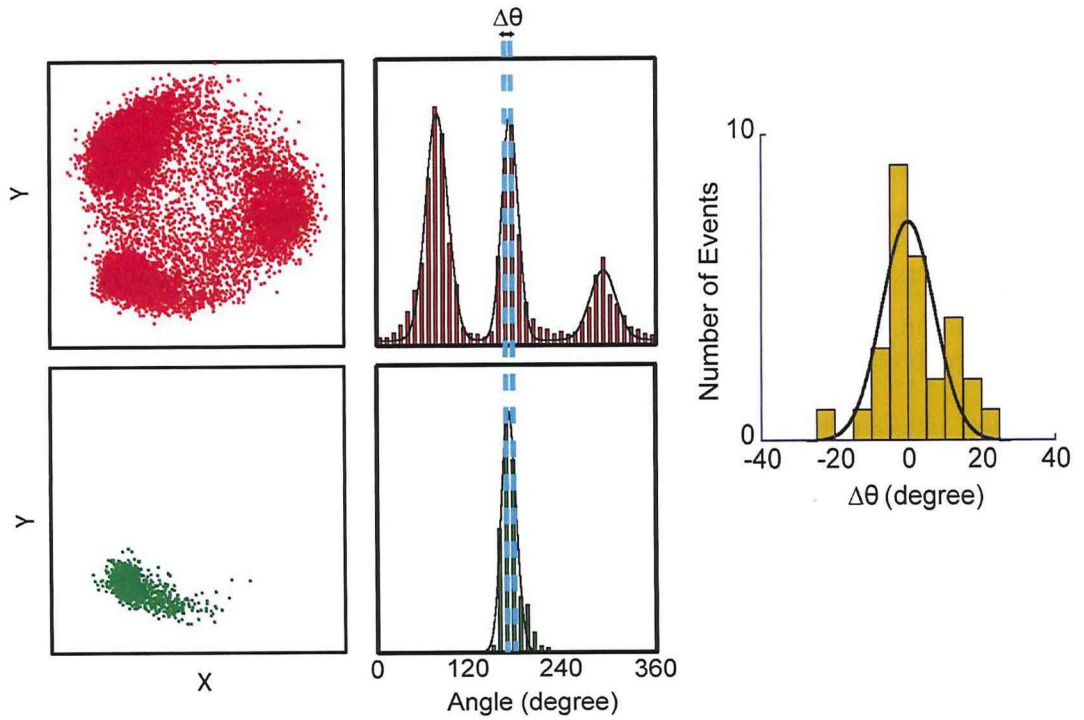

Figure 18. Long pause shares the same angular position with short pause (38). By observing rotation of a single molecule until it lapses into long pause, angular positions of both pauses were compared. Until the molecules lapse into long pause, short pauses were noticed at saturating [ATP].

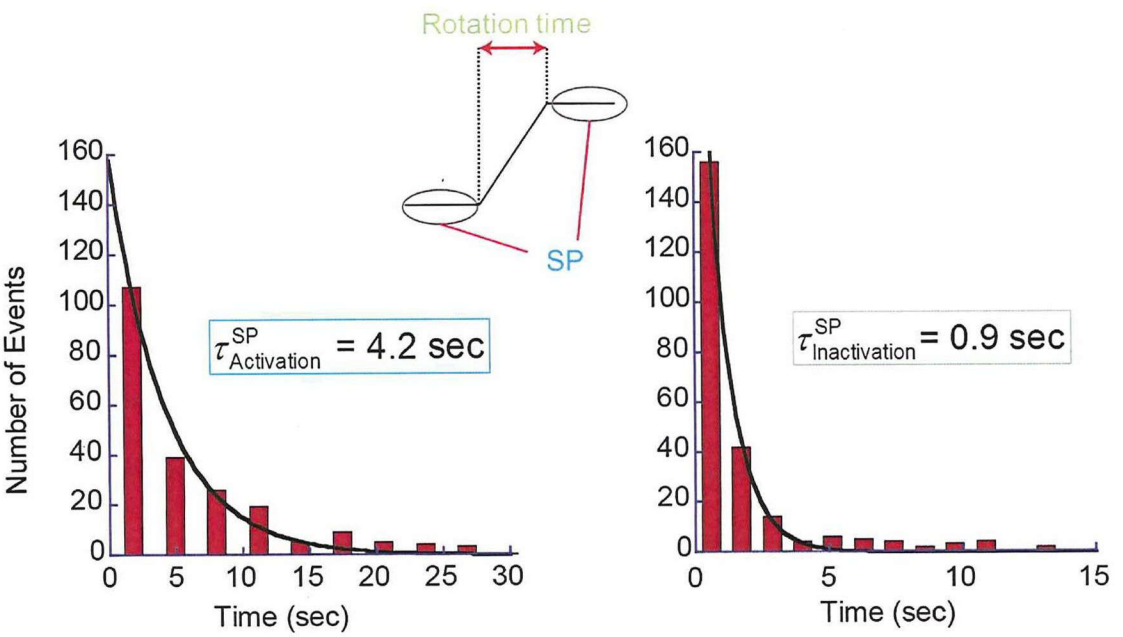

Figure 19. Time constants of short pause and rotation time between two successive short pauses were determined from dwell time analysis. V_1 molecule rests for ≈ 4 x rotation time (38). V_1 molecule rests more than works.

As a means of comparison, we measured the time-dependent inactivation in bulk ATPase assay under the presence of ATP-regenerating system. As previously reported, (5,36), the ATPase activity was gradually inactivated and finally reached nearly zero in 80 min. This time-dependent inactivation is explained by ADP inhibition: V_1 fails to release ADP produced upon hydrolysis and transforms into the stable inhibitory state. Fitting the time course with a single exponential function gave the time constant of 3.4 min. Although this time constant is in the range of minutes, similar to $\tau^{LP}_{Inactivation}$ (17.6 min), it is evidently faster than $\tau^{LP}_{Inactivation}$. However, if we look carefully to the time course of inactivation in bulk ATPase assay, we can see there are two phases, fast inactivation process which is followed by slow inactivation (cyan-dotted line). This finding suggests that there are two independent pathways for reaching ADP inhibition. When we fitted the time course from bulk ATPase assay with double exponential, we obtained two time constants of 2.13 min and 15.7 min. From the equilibrium level of fitting, the equilibrium constant of inactivation was calculated to be 0.018, which gives the energy difference between active state and LP as -4.0 k_BT.

Rotation time constant determined from dwell time analysis of single molecule analysis is 17.6 min. However, the bulk ATPase assay gave us a different value for rotation time, 3.4 min (from single exponential fitting). Even though the units are matching, the values are quite different. When we look at the bulk ATPase assay graph carefully, we could distinguish that there are two populations, fast-living V_1 and slowly (long)-living V_1. Double exponential fitting gave a time constant for long-living V_1 as 15.7 min similar to that obtained from single molecule analysis (17.6 min). The later time constant (15.7 min) is quite close to

$\tau^{LP}_{Inactivation}$, which implies that the slow inactivation process leading to the *LP* state corresponds to the slow inactivation observed in the bulk ATPase assay. One reasonable explanation for why we could not observe fast-inactivating molecule during rotation assay could be that the molecules inactivated via the fast pathway stopped rotation before being identified under optical microscope; because the probability of finding actively rotating wild-type V_1 particles is quite low compared with the TSSA mutant of V_1 that was often used for kinetic analysis of V_1 rotation (4,14,35-37,42,43). In case of wild-type V1, over 5 min was usually required to find the first rotating particle after ATP infusion into the flow cell.

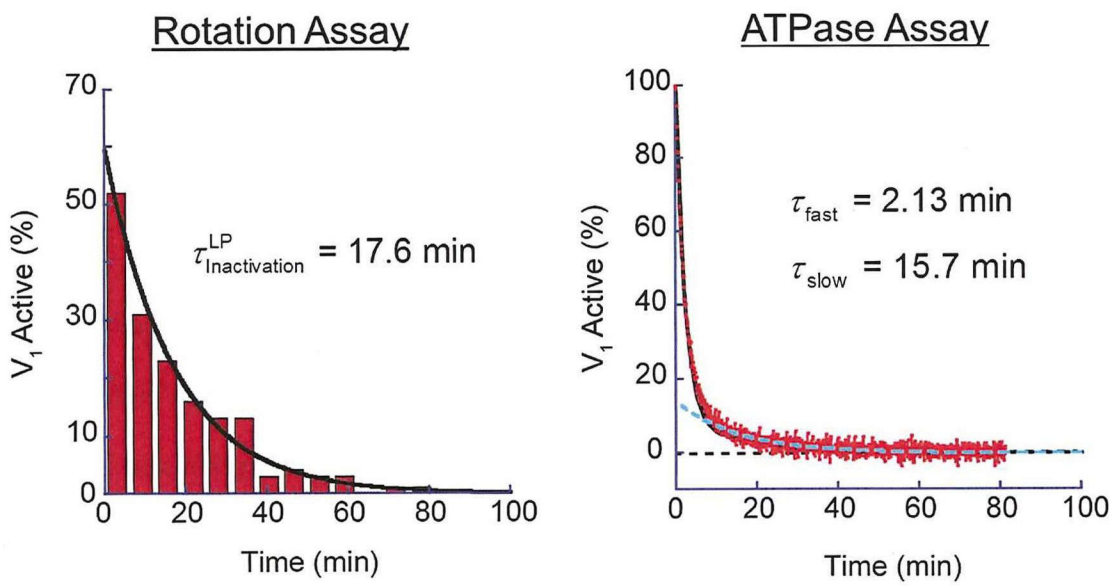

Figure 20. Rotation time of single V_1 molecules until lapsing into long pause, determined from single molecule assay and bulk ATPase assay (38).

2.4 Viscous load effect on pausing behavior

So far, we demonstrated the existence of short and long pause, and analyzed their characteristics in rotation assay by using a quite big magnetic bead. However, we need to

check the effect of viscous drag on kinetics of these pauses. For this purpose, we decided to use a really small bead (40 nm gold colloid) which shows negligible viscous drag much lower than that of the magnetic beads (17). However, even in drag-free condition, V_1 showed transient, second-scale short pauses and final long pause (Figure 21).

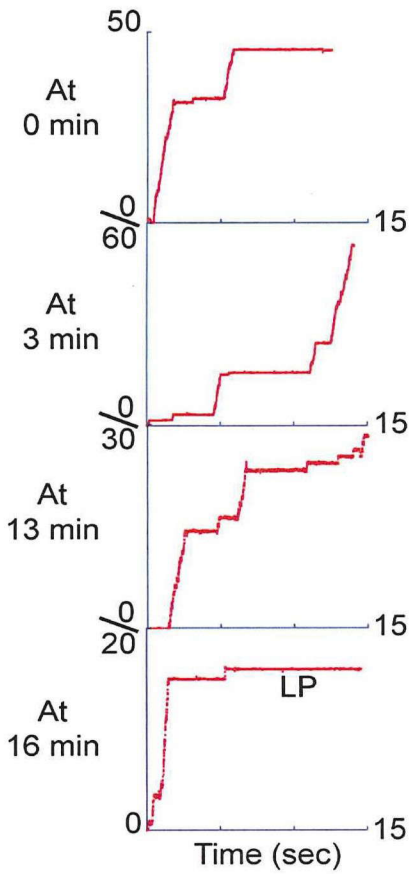

Figure 21. Rotation of a single molecule attached to 40 nm gold colloid (38). Due to the big file size, we recorded the molecules at every 3-4 min for min of 10 sec. Rotation was recorded with high-speed camera. Here, recording rate was 250 frame/sec. Transient pauses which last for several seconds were observed, these represent the short pauses that we have observed in case of magnetic bead. The long pause was also observed, after several times of recording the same molecule.

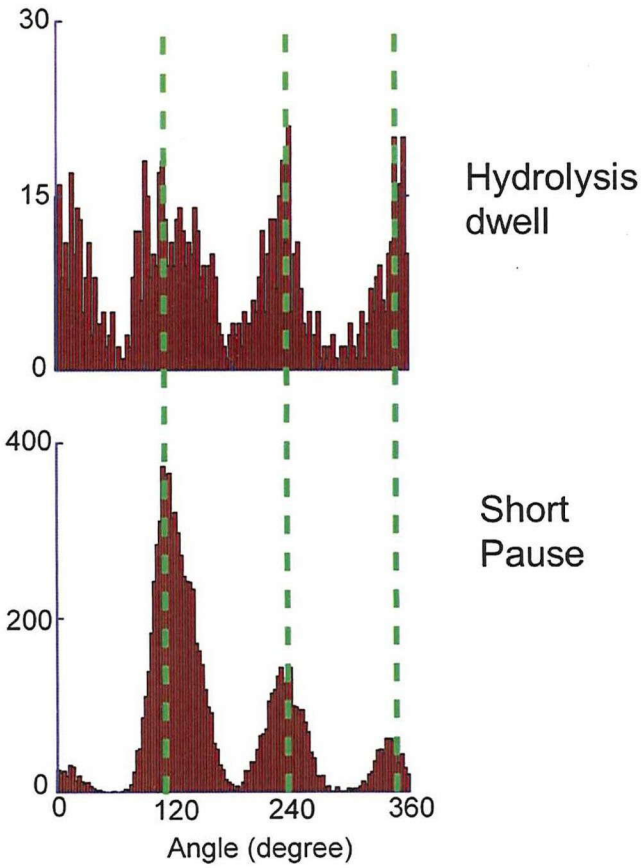

Figure 22. Short pause share the same angular position with catalytic dwell (38). The above histogram was obtained by analyzing the very short dwells observed during rotation time. And short pauses were defined as longer than one second.

Because of the smaller load size, V_1 motor reached max speed of 64 rps, at saturating, 4 mM ATP. To catch-up with the rotation speed of V_1, we used high speed camera for recording. The min time resolution that we used during recording was 4 msec. At this resolution, we could distinguish the sum of two dwells (5 ms) due to ATP-cleavage (2.5 ms) and one (or both) of product release (2.5 ms) (17). ATP-waiting dwell was 0.3 msec, indistinguishable under this resolution. The angular distribution of rotating time between two successive short pauses should reflect this 5 msec interval, and indeed we saw 3 angular positions separated by 120°. Then we compared the angular positions of this 5 msec joint dwell with

that of short pause, the positions of these two events overlapped (Figure 22). Previous literature reported that ATP hydrolysis occur at the same angle with ATP waiting (15,17). This observation again supported our finding that short pause and ATP binding share the same angular position.

Then we calculated the mean time constant for short pause and rotation time between two successive short pauses as 3.50 ± 0.54 s (48 events) for $\tau^{SP}_{Activation}$ and 0.55 ± 0.24 s (36 events) for $\tau^{SP}_{Inactivation}$. These values are consistent with those obtained from magnetic bead case.

We attempted to determine the rotation time until lapsing into long pause. However, due to the big file size, we could not record rotation with fast framing camera over 5 min. Therefore we performed a time-lapse rotation assay; every 3–4 min, we recorded the rotary motion of the targeted molecule with a fast-framing camera for at least 10 s. With this method, the final long pause was observed. Even though the time resolution was around 3 min, the average rotation time before *LP* was calculated to be 16.7 ± 7.8 min (6 molecules). This observation is also consistent with our previous calculation based on magnetic bead rotation assay.

Herein, we confirmed that the viscous drag does not affect the kinetics of pauses. From now on, we again used the magnetic bead as the rotation marker in the single-molecule rotation assay.

2.5 Effect of solution ADP and inorganic phosphate on the pauses

Previous studies about F_1-ATPase showed that addition of ADP into reaction mixture of rotation assay caused immediate stop of rotation due to being trapped in ADP-inhibited state (30). We wanted to investigate whether a similar effect would be seen for V_1, so we injected 200 μM ADP into chamber solution together with ATP. This amount of ADP was

reported be enough to inactivate V_1 after pre-incubation with ADP (5). To our surprise, a clear effect of ADP was not observed on the rotation behavior of V_1. Kinetic parameters of short pause, $\tau^{SP}_{Inactivation}$ and $\tau^{SP}_{Activation}$ were not essentially affected by ADP (Table 1). The duration time of rotation until *LP*, $\tau^{LP}_{Inactivation}$ also did not change (Table 2).

	4 mM ATP$^{\gamma}$	30 mM NaPi$^{\gamma}$	200 μM ADP
Short Pause (sec)	**4.2** ± 0.3	**4.4** ± 0.4	**4** ± 0.3
Rotation Time (sec)	**0.9** ± 0.04	**1.7** ± 0.1	**0.8** ± 0.02

*All experiments are performed in the presence of 4 mM ATP.

$^{\gamma}$ATP regenerating system is supplied.

TABLE 1. Dwell times of Short Pause and Rotation Time obtained from single exponential fitting of dwell histograms. Number of molecules and number of events used in this analysis were as follows: 4 mM ATP: 7 mols, 250 events; 30 mM NaPi: 3 Mols, 130 events and 200 μM ADP: 4 mols, 170 events.

	4 mM ATP$^{\gamma}$	30 mM NaPi$^{\gamma}$	200 μM ADP
Life Time of Rotation* (min)	17.6 ± 1.5	14.8 ± 1.7	15.8 ± 2.6

* Mean ± Std. error

$^{\gamma}$ATP regenerating system is supplied.

TABLE 2. Rotation time until *LP* under saturating [ATP], [ADP] or [Pi]. All experiments were

done in the presence of saturating [ATP], 4 mM. The number of molecules used and the total number of events for different conditions were as follows: 4 mM ATP: 98 mols, 164 trials; 30 mM NaPi: 43 mols, 72 trials; 200 μM ADP: 35 mols, 67 trials.

Next, we wanted to test the effect of inorganic phosphate (Pi) because solution Pi somewhat rescues F_1 from ADP-inhibited state. However, solution Pi neither affected the kinetics of the pauses.

These data suggest that short pause state is irrelevant to the ADP-inhibited state. Against our expectation, rotation time until LP was similarly not affected by solution ADP. One remaining possibility is that the reverse reaction rate, the activation from LP could be dependent on solution ADP. However, the duration time of long pause is too long to be analyzed without disturbance. So, we tested this possibility by using magnetic tweezers (next section).

2.6 Mechanical Activation from LP State

The kinetic features of LP do not match perfectly with those of ADP-inhibited state of V_1 from bulk ATPase measurement (5). However the basic characteristics of LP such as its time scale and apparent irreversibility support the contention that LP corresponds to ADP-inhibited state of V_1.

In the case of F_1, ADP-inhibited state was mechanically activated by applying external force: when F_1 in the ADP-inhibited state is forcibly rotated in forward direction by 80°, it always resumes active rotation immediately after release from the external force (1).

We were curious whether V_1 in LP could be also activated by external force similar to ADP-inhibited F_1. A schematic image of the experimental setup for applying magnetic field was

shown in Figure 11: In this experiment, magnetic bead was not only used as the rotation marker but also as the handle to control angular position of rotary shaft of V_1. The torque for external control was generated with magnetic tweezers which is composed of crossly located two pairs of electromagnets and is mounted 1 cm above the microscopic stage. Magnetic tweezers generated a magnetic field parallel to the stage, and the magnitude and orientation of the magnetic field could be controlled by the electric current on each electromagnet.

Before applying a magnetic field to V_1, we had to ascertain that molecule lapsed into LP state. So far-observed, the longest short pause was around 4 min. Therefore, we set our criteria for LP as a pause longer than 5 min while dwelling at one of the three *SP* angles. After waiting for 5 min, a magnetic field was applied to forcibly rotate the V_1 molecule in LP and stall it at a target angle. After the set time period passed, we switched off the current to release the molecule from magnetic field. Similar to the mechanical activation of ADP-inhibited F_1 (1), V_1 showed essentially two behaviors. One is the reactivation from LP state. V_1 resumed active rotation immediately after released from the magnetic tweezers. Once reactivated, V_1 made a continuous rotation until being trapped in the SP state. The rotation velocity after reactivation was same as that before entering into LP state. These findings imply that V_1 reactivated from the LP state completely resumed the catalytic activity of ATP hydrolysis. The other type of response to the manipulation was the return to the original pausing angle after release from the magnetic field. In this case, V_1 again showed LP unless activated by another manipulation. Examples for typical time courses of the reactivation and the failure of reactivation were shown in Figure 23.

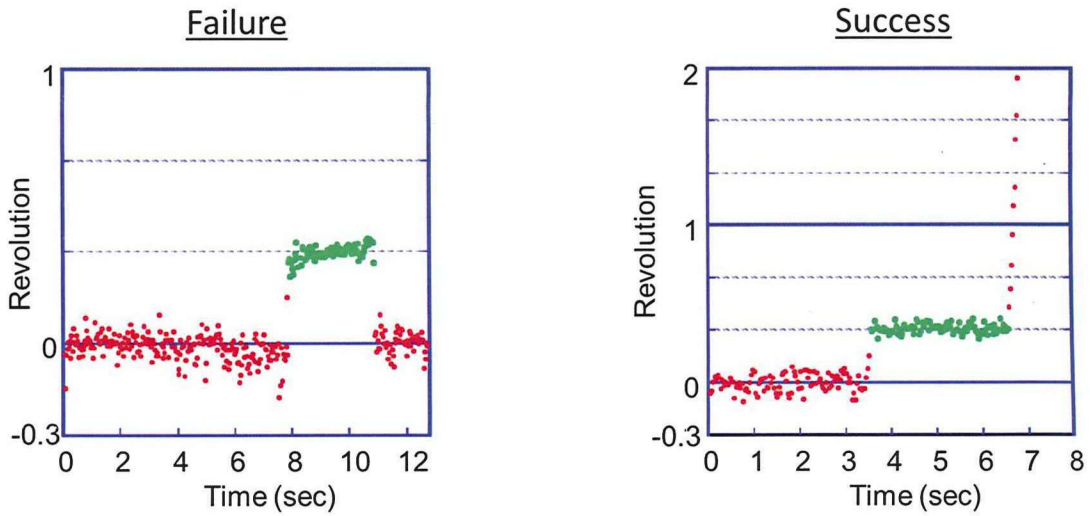

Figure 23. Typical behaviors of V_1 upon release from the tweezers (38). One is failure (left) and the other is success (right) in reactivation.

Unclassifiable behaviors were also observed (less than 1%). The typical behavior of the minor events was that the molecule returned to the original angle after release from the magnetic field and resumed rotation spontaneously within 30 s, which is too short to be classified as LP. In this case, V_1 most probably changed the pausing state from LP to SP upon the manipulation. This type of data was omitted from the data analysis.

2.6.1 Angle dependency of Mechanical reactivation

We stalled V_1 in the *LP* state at angles ranging from –110° to +110° for 10 sec, at 4 mM ATP (38). Based on these manipulations, we calculated the reactivation probability (%) defined as the ratio of reactivation events to the total number of trials. As seen in Figure 24, reactivation was never observed in clockwise direction. Even in the counterclockwise direction, until 50°, none of the molecules were reactivated. Manipulation over +50° induced reactivation. When the magnetic bead was rotated +110°, most molecules resumed active

rotation just after being released. With this experiment, we confirmed that V_1 paused in the *LP* state can be reactivated with forcible forward rotation similar to F_1 under ADP inhibition.

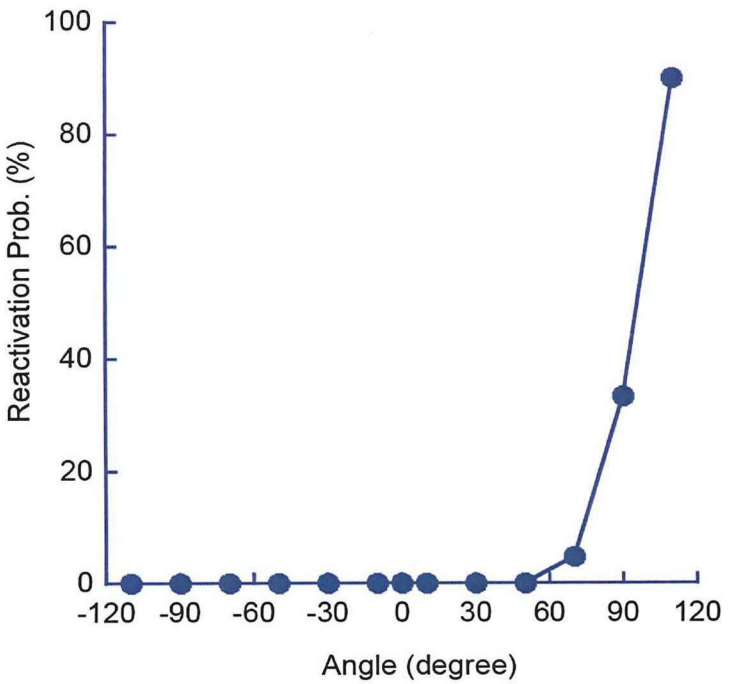

Figure 24. Reactivation probability against stall angle (degree) (38). In counterclockwise direction, reactivation from LP was never observed. Starting from +50 degree in clockwise direction, reactivation probability increased and reached its max value at +110 degree.

2.6.2 Suppression by ADP

Next, we wanted to test the effect of solution ADP on the reactivation of V_1 in the *LP* state (38). We previously showed that solution ADP didn't affect any of the following parameters: SP, rotation time between SPs and rotation time until LP. Subsequently, we would like to see if the reactivation rate from LP will be affected.

And in the case of F_1, solution ADP was shown to suppress the reactivation of F_1 under ADP inhibition.

The reactivation probability was determined in the presence of 200 μM ADP and 4 mM ATP. The suppressive effect of ADP was evident at +110° and +90°, but was not observed at +70° (Figure 25). The reactivation probability at +110° decreased from 90% to 31%. Thus, reactivation from the *LP* state was also found to be sensitive to solution ADP, as we expected from the contention that *LP* represents the ADP-inhibited form of V_1.

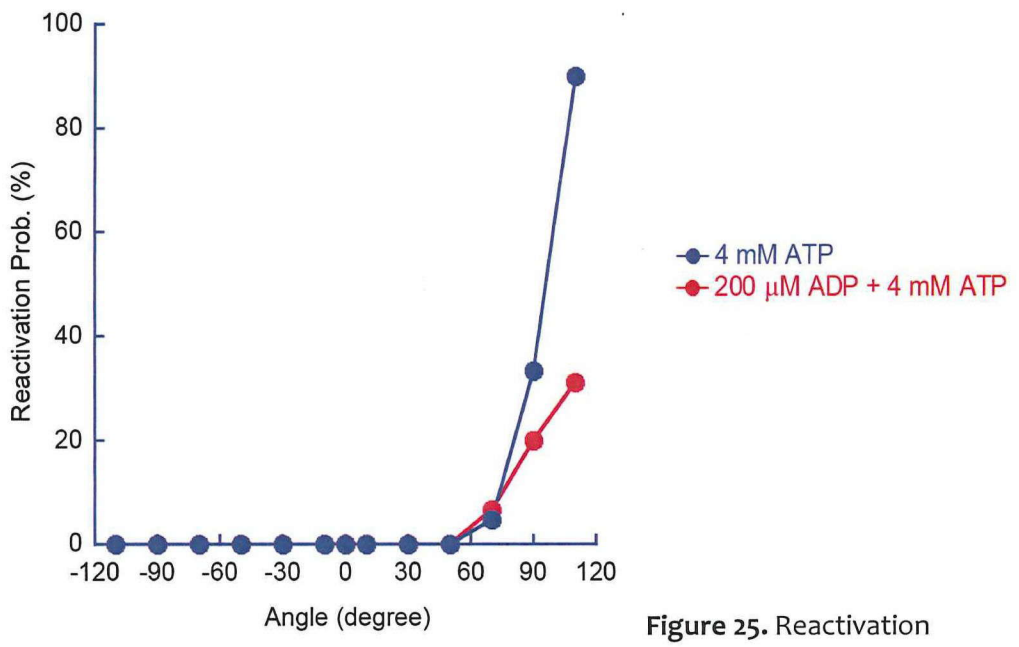

Figure 25. Reactivation probability against stall angle in the presence of saturating [ADP] (38). Effect of ADP was clearly observed at stall angles of 90 and 110 degree. At 110 degree, reactivation probability decreased from 90% to 31%.

2.7 Discussion: Comparison with F_1

2.7.1 SP in V_1 and F_1

Bulk ATPase assay of *T. thermophilus* V_1 suggested that V_1 decreases ATPase activity with time constant of 3.4 min until the activity almost reached zero. Inactivated V_1 tightly binds

ADP at the catalytic site and it does not resume activity until bound ADP is removed. Actually during the purification process of V_1-ATPase, we apply a method to remove the bound ADP, which results in drastic increase of mean ATPase activity. However, even after repetition of this method for several times, a significant portion (17%) of the molecules were still bound ADP. The SP state was the most frequently observed pause during the rotation. However SP cannot represent the biochemically suggested ADP inhibition because its time constants of inactivation and activation ($\tau^{SP}_{Inactivation}$ = 0.9 s and $\tau^{SP}_{Activation}$ = 4.2 s) are both too short. So, SP is a newly identified inhibitory state of V_1.

SP can neither be an artifact possibly caused by viscous drag of the big rotation probe (magnetic bead), because rotation with essentially drag-free probe (40 nm gold colloid) still showed SP. The occurrence frequency and its lasting time were both consistent with those obtained from magnetic bead case. Actually a similar short pause of a second-scale dwell time (1.7 sec) was reported for F_1-ATPase (30). But the physiological role and the mechanism of short pause in both motors are not identified (Figure 26). Further study should be done.

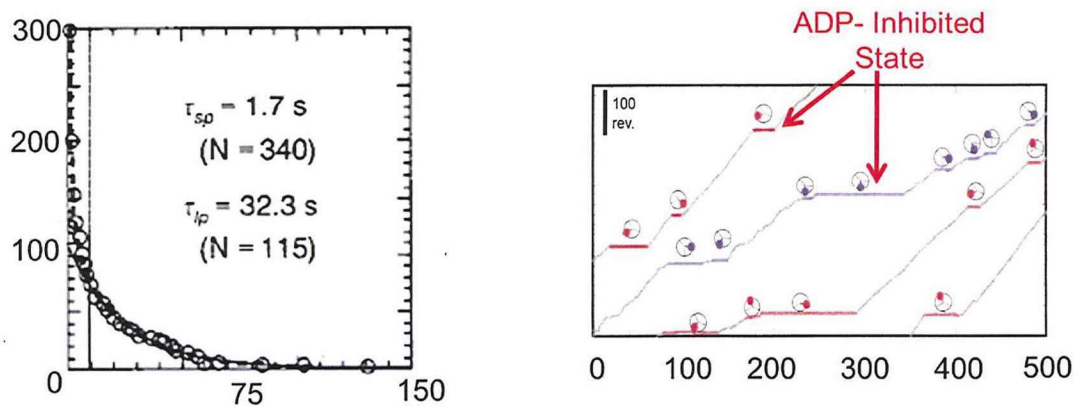

Figure 26. Two types of pauses observed in F_1-ATPase (left) (30). 30-sec pause corresponds to ADP-inhibited state of F_1. The trajectories on right show the 30-sec pauses (colored parts). However, the 2-sec pause was not attributed to any catalytic state of APT hydrolysis. Further research is necessary to deduce the role of SP and 2-sec pause in V_1 and F_1, respectively.

Another interesting point is that we didn't see clear second-scale inactivation or activation caused by SP in bulk ATPase assay. Actually a slight activation was observed at the beginning of ATPase activity assay (5), however degree of activation is quite small as compared to activation rate from short pause. These findings imply that SP state involves some conformational rearrangement that is not related to catalysis. So, V_1 probably is in equilibrium between the active state and SP state before being injected into assay mixture for bulk ATPase measurement. Actually this assertion somehow explains the marked discrepancy of the bulk ATPase rate and rotation speed from single molecule rotation assay. Rotation speed is clearly faster than that expected based on bulk ATPase rate. Even though the rotational rate of V_1 at V_{max} condition was reported to be 64 rps, the value estimated from bulk ATPase rate (1/3 of ATPase rate) was only 12 rps. Based on activation rate from SP state, estimated fraction of active V_1 at any time is only 18%. If we correct bulk ATPase rate assuming that only 18% of the V_1 molecules are in active state, then the genuine rotation rate would be 67 rps, which is almost same as the actual rotation speed from single-molecule assay. This calculation is in favor of above assertion mentioning the pre-existing equilibrium between the active and inactive states.

Moreover, we showed that solution ADP does not have any effect on either SP or rotation time between SPs. This finding also supports that SP state is irrelevant to catalysis, and very clearly not related to ADP binding.

2.7.2 LP of V_1 is more stable than that in F_1

Bulk ATPase assay pointed out that *LP* state has an expected minutes-scale inactivation time

constant. The extremely long duration time of the *LP* state obtained from single-molecule assay is consistent with the prediction from the bulk ATPase assay. Actually, ADP-inhibited state is so stable that V_1 almost completely lost its catalytic activity, suggesting that the time constant of reactivation is very big. This finding is in contrast to the ADP-inhibited form of F_1-ATPase (Figure 27), which spontaneously resumes active rotation after 30 s under the assistance of thermal agitation (30).

During the mechanical manipulation, LP of V_1 required stalling over >50° for reactivation, though F_1 reached almost 70% reactivation probability at 50° (Figure 28). This suggests that activation energy for the activation of ADP-inhibited V_1 is much larger than that for F_1.

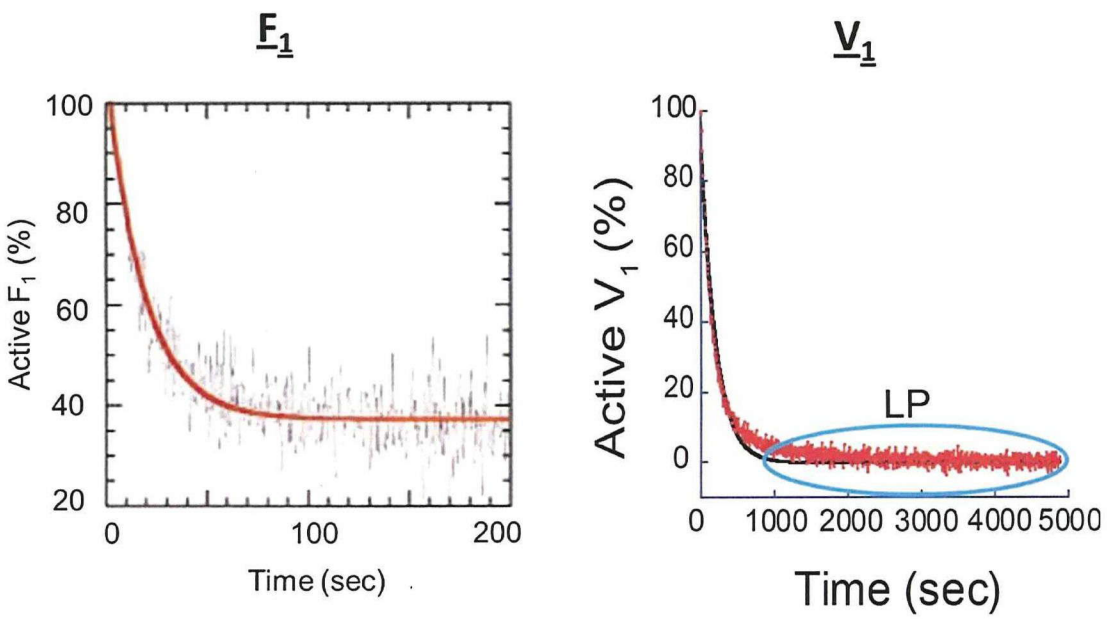

Figure 27. Time course of activity of F_1 (left) and V_1 (right) (30,38). Even though all V_1 molecules finally lapse into long pause state, only 60% of F_1 molecules gained ADP-inhibited state.

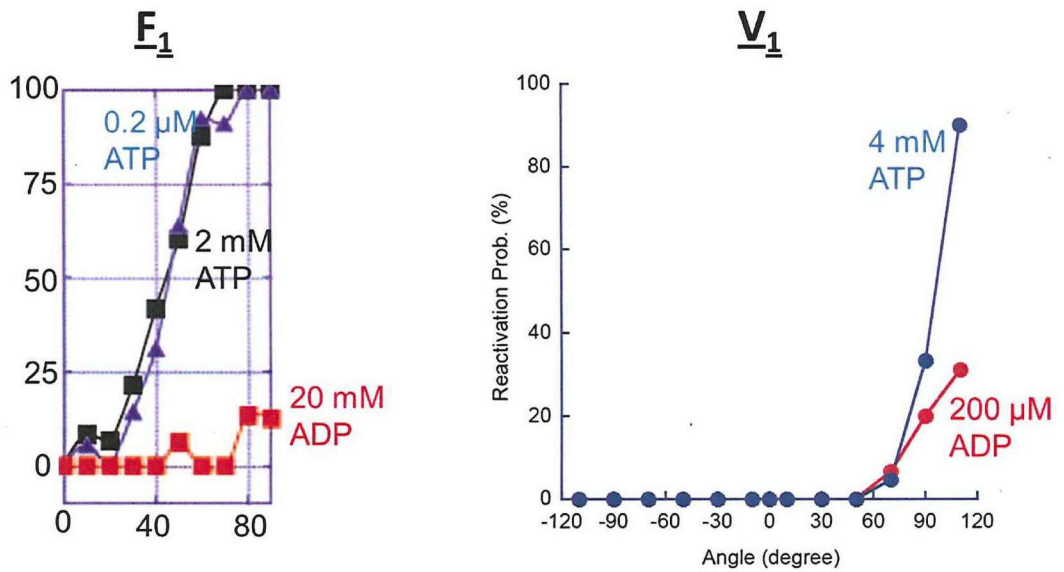

Figure 28. Reactivation probability against stall angle under varying buffer conditions: For F_1, 0.2 μM ATP, 2 mM ATP and 20 mM ADP (+33 μM ATP) (1). For V_1, 4 mM ATP and 200 μM ADP (+ 4 mM ATP) (38). Reactivation probability achieved at 70° is almost 100% in case of F_1, though less than 10% in case of V_1.

2.7.3 Physiological role of SP and LP

The energy differences of SP and LP state from active states are -1.5 and -4.0 kBT, respectively. These states are significantly stable as compared to that of ADP inhibition of F_1 (-0.6 kBT). This finding implies that free V_1 takes a longer rest than F_1 during pausing of the catalytic turnover.

Based on current findings of this study, we could not determine the physiological role of SP. However, we could simply hypothesize that both SP and LP states are dual suppression mechanisms for free V_1 motor to escape from wasteful consumption of cellular energy source, ATP. Isolated V_1 was found in the *T. thermophilus* cytosolic fraction. And it is well known that yeast V_1 domain detaches from the whole complex upon glucose starvation, and upon detaching, isolated V_1 somehow lost its ATPase activity. We don't have any

knowledge whether yeast V_1 has similar pausing states, SP and LP, like *T. thermophilus* does. Further study on rotation of eukaryotic V_1 is necessary.

2.8 Conclusion

For studying the individual reaction steps during ATP hydrolysis, single-molecule rotation assay was held. Some pausing behavior of V_1 was observed, during rotation assay. To be able to continue with our goal of manipulating individual reaction steps, first we needed to characterize these pauses.

V_1-ATPase indicated two types of pauses during rotation, one was a reversible, second-scale 'short pause', and the other one was an irreversible 'long pause' which marks the end of rotation.

Short pause was a newly found inhibitory state, though long pause was previously predicted from bulk ATPase assay. Our single molecule analysis supported that long pause represents the ADP-inhibited state of V_1. In case of F_1, ADP-inhibited state is reversible, which suggests that V_1-ATPase is more strictly controlled than F_1-ATPase.

V_1-ATPase in long pause was reactivated when the shaft was forcibly rotated above 50° in forward direction via the magnetic bead. The observed angle dependence of long pause was distinctive from that of F_1-ATPase, implying that energetic and kinetic features of mechanochemical coupling of V_1 are different from those of F_1.

Chapter 3. Mechanical Modulation of ATP Binding Affinity

After characterization of the pausing states of V_1, we wanted to focus on ATP binding event in ATP hydrolysis cycle (Figure 12). By using the magnetic tweezers setup like in case of LP state, we applied magnetic field to central shaft during the waiting time for binding ATP. Results of mechanical manipulation were explained below. The contents of this chapter will be soon submitted to a journal for publication.

3.1 3-step rotation at non-saturating [ATP]

Same setup from Chapter 2 was used here for rotation assay and mechanical manipulation: For rotation assay, a streptavidin-coated magnetic bead was attached to D subunit of central shaft. Here, magnetic bead was used also as a handle for manipulating the rotary shaft. Rotation assay was conducted under ATP-limiting conditions (1 or 1.5 μM), well below the Michaelis-Menten constant (K_m) of the rotation assay with magnetic beads (8.1 μM). At these ATP concentrations, V_1-ATPase demonstrated a 120° stepping rotation (Figure 29). The mean times of the ATP-waiting pause were 0.57 and 0.32 sec at 1 and 1.5 μM, respectively. We should keep in mind that mean time for catalysis on V_1-ATPase was 2.5 msec, which is much shorter than ATP-waiting dwell and mean time for 120° rotation of the beads. So, catalytic pause was undetectable in this condition.

3.2 Mechanical Manipulation during ATP binding dwell

Under non-saturating ATP concentrations such as 1 μM ATP, occurrence frequency of second-scale short pause was less than 0.4% of the total pause and therefore its effect is negligible as compared to ATP-waiting dwell.

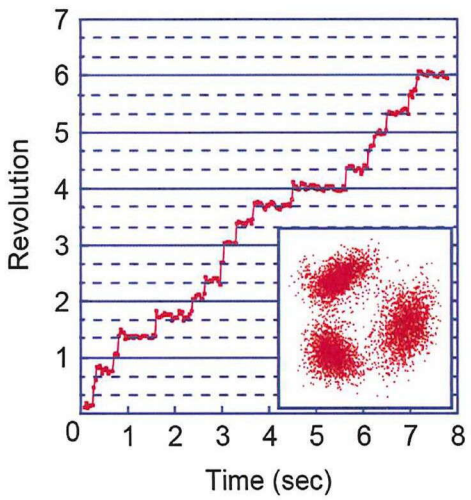

Figure 29. Rotation trajectory of a single molecule, in the presence of 1 μM ATP. The pauses are the ATP-waiting dwells. Inset shows the X vs Y trajectory of this molecule. 120° stepping behavior was clearly observed under [ATP] less than K_m.

When V_1-ATPase paused for binding ATP, magnetic tweezers was turned on to stall magnetic bead at a target angle. After the set period of time passed, magnetic tweezers was turned off to release the magnetic bead and therefore the shaft of the molecule. Upon our manipulation, in general two behaviors were observed, similar to in case of long-pause state (38). One type of response was going to next ATP-waiting angle immediately after release. V_1-ATPase cannot rotate to the next stepping angle unless it binds ATP. This means that when the molecule was released, it was already bound to ATP. This response was named as 'on' event. The other response was going back to the original waiting angle just after release from the tweezers. In this case, the molecule was not bound ATP at the time of release, therefore it couldn't generate the torque needed for rotating to the next step and just returned back to the angular position where it came from. This second response was named as 'off' event. Some unclassifiable responses were also observed; for instance the molecule went back to the original angle after release from the magnetic field, like in

the case of an 'off' event however didn't resume the rotation anymore. In this case maybe the molecule lapsed into long pause state. This type of behaviors was rarely encountered (less than 5%), therefore discarded from analysis.

The waiting times just after manipulation were analyzed to check whether our mechanical manipulation results in change of any kinetic or catalytic properties of the enzyme. In case of an 'off' event, dwell time after coming back to original angle until spontaneously binding ATP was analyzed (Figure 30). And for the 'on' event, dwell time of ATP binding on the next stepping angle was analyzed (Figure 30). In both cases, the dwell time histograms gave close values to original ATP waiting time constant (0.57 sec) from free rotation at 1 μM ATP. This implies that stall-and-release type of mechanical manipulation affected neither catalytic nor kinetic properties of V_1-ATPase, suggestive of the high robustness of this enzyme.

After many trials of manipulation, the probability of ATP binding was measured as the probability of an "on" event, P_{on}.

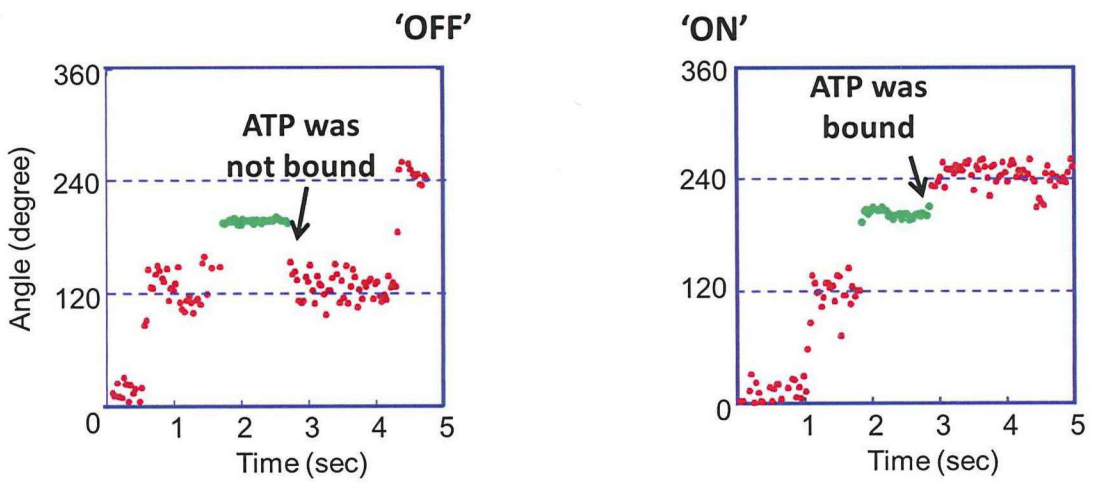

Figure 30. Two typical behaviours of V_1-ATPase upon mechanical manipulation during ATP binding dwell. One is the molecule returns back to the original angular position after release from the tweezers, 'off' event. The other is the molecule jumps to the next stepping angle directly from the stall angle position upon release, called as 'on' event.

3.2.1 Angle and Time dependency of P_{on}

P_{on} obtained at non-saturating 1 μM ATP was plotted against the stall angle, for stall times of 0.5, 1, 3 and 6 sec (Figure 31). Stall angles were varied between -100° and +100°, with increment size of 40°. Here, 0° was assigned as the mean angle for ATP-waiting pause and the plus direction, same as direction of free rotation (counterclockwise). P_{on} increased as the stall angle increased, reaching its maximum value at 100degree. In the angle range of [-60°, +60°], stalling longer than 0.5 sec resulted in a significant increase in P_{on} (%). However, above 1 sec stalling, P_{on} values did not significantly change depending on stall time. This result was in good agreement with our expectation such that at stalling above ≈0.6 sec, P_{on} values should reach saturation. Time constant for ATP binding during free rotation is 0.57 sec. So stalling longer than the threshold, 0.57 sec, should give saturated values for P_{on}.

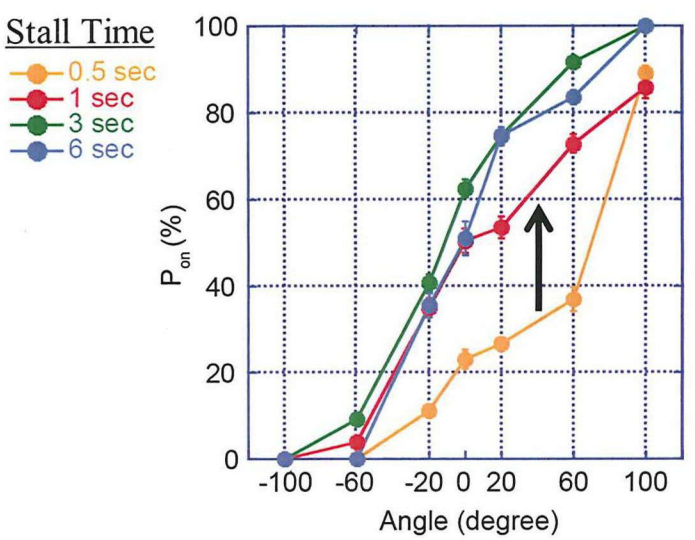

Figure 31. P_{on} against stall angle, at different stall time conditions under 1 μM ATP. Stall times used in this experiment were displayed next to the graph. A clear difference between the P_{on} values of 0.5 sec and above 0.5 sec could be seen.

To see the time course of P_{on} for varying stall angles, the data points were re-plotted against the stall time (Figure 32). From the graph, we omitted data of -100°, because they

were extremely low to provide a reliable time-dependent progress for P_{on}. As seen in the Figure, time courses reached saturation at around 3 sec. Another important point is that saturation was below 100%, at all stall angles except +100°. This suggests that ATP binding during stalling was reversible. If we stall the molecule for long time period, during our stalling, the molecule not only binds ATP but it also releases bound ATP into environment. This was also observed in case of stall-and-release experiment performed for ATP binding event in F_1-ATPase (21).

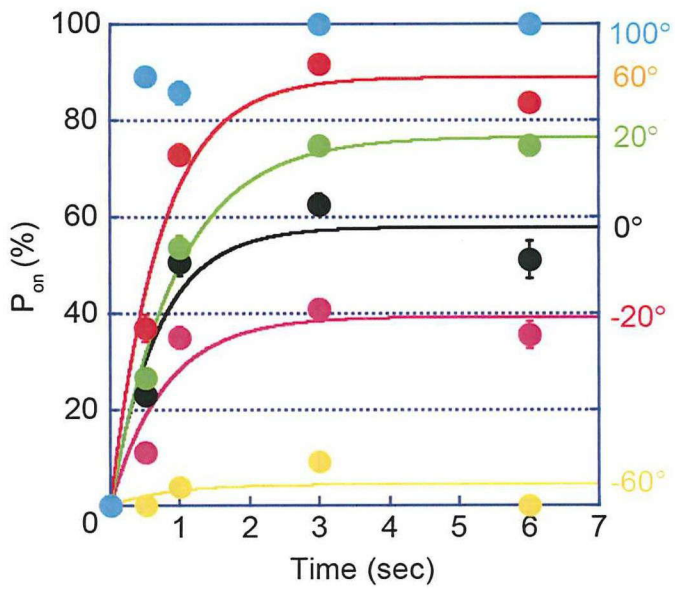

$$V_1 + ATP \underset{k_{off}}{\overset{k_{on}}{\longleftrightarrow}} V_1 \cdot ATP$$

$$P_{on} = \left(\frac{k_{on}}{k_{on} + k_{off}}\right)\left(1 - \exp[-(k_{on} + k_{off}) \cdot t]\right)$$

Figure 32. Probability of 'on' event against stall time. The same dataset from Figure 31 was used to draw this graph. Time course of ATP binding depending on stall angle can be clearly observed. After 3 sec, P_{on} seemed to saturate regardless of stall angle. Except +100°, P_{on} of other stall angles saturated below 100%, implying that ATP was also released during our mechanical manipulation.

3.2.2 Rate constants of ATP binding and release

We fitted the time course of P_{on} based on a reversible reaction scheme. From the fitting, we determined the rate constants of ATP binding and release. The dissociation constant of ATP was also determined from the ratio of k_{off} to k_{on}. We plotted these rate constants against stall angle in semi-log scale (Figure 33). k_{on} increased exponentially upon V_1-ATPase rotation, whereas k_{off} reduced exponentially. Between [-60, +60] angle range, k_{on} increased by approximately 22 fold, while k_{off} decreased by 8 fold, which resulted in the decrease of K_d by approximately 173 fold.

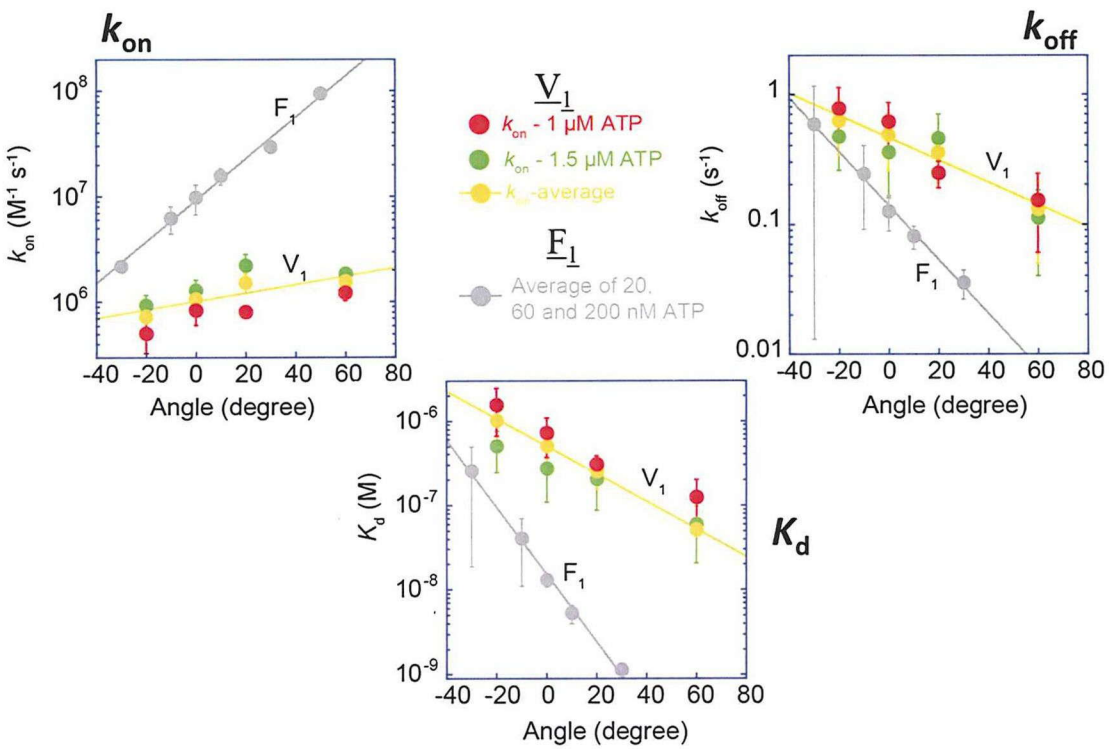

Figure 33. Rate constants of ATP binding (k_{on}) and release (k_{off}) were determined from the fitting of P_{on} vs time graph. K_d was derived from the ratio of k_{off} and k_{on}. F_1 data is courtesy of Dr. Rikiya Watanabe (21).

As seen from the graph, ATP-binding rate determined from free rotation is slightly higher than k_{on} at 0° which was determined from stall-and-release experiment. This situation was also observed in case of F_1-ATPase. This observation could be explained by rate enhancement due to the thermal agitation; rotary shaft is subject to rotary fluctuation due to thermal noise. When an infrequent large rotary fluctuation occurs in forward direction (counterclockwise), ATP binding event takes place.

3.2.3 Calculation of torque generated by ATP binding

Angle dependency of kinetic parameters could give us information about torque generation driven by ATP binding. Rather than the individual data points, general tendency of kinetic parameters over an angle range is important. The study done on F_1-ATPase estimated the torque contribution by ATP binding from the angle dependency of k_{off} (21). Then they compared this value with that of ATP-hydrolysis event.

Torque generated by ATP binding corresponds to slope of rotary potential of ATP-bound state (Figure 34) (16). Relative energy difference between the ATP-bound state and the transition state for ATP binding/release was given by the formula, $-k_B T \ln k_{off}(\theta)$. Differentiation of this formula with respect to angle, $-k_B T \frac{\partial[\ln k(\theta)]}{\partial \theta}$, gives us the torque generated by ATP binding. Here we assume that only free energy of ground state changes upon rotation, while activation energy remains constant over defined angle range. So, by using this formula, we calculated the torque generated by ATP binding as 4 pN·nm for V_1-ATPase. The whole torque by hydrolysis of a single ATP molecule is 35 pN·nm. So, contribution by ATP binding event to whole torque is only 11%. However, we should keep in mind that these torque values must be underestimated due to the elasticity of the experimental setup.

Torque $\left(\frac{\text{pN nm}}{\text{radian}}\right)$		F_1	V_1
	ATP binding	‡11	4
	Total	Ω40	Ψ35

ΩNoji, *et al.* (1999) *BBRC*
ΨImamura, *et al.* (2005) *PNAS*
‡Watanabe, *et.al. (2011) Nat.Chem. Bio.*

Figure 34. Torque generated by ATP binding was calculated from the slope of rotary potential of ATP-bound state. Torque by ATP binding in V_1 was found to be 4 pN·nm, which is 11% of whole torque (35 pN·nm) by hydrolysis of a single ATP molecule (15).

3.3 Discussion and Comparison with F_1

3.3.1 Is ATP binding not the primary torque generating step?

A previous study, by performing the same stall-and-release experiment, determined the rate constants, k_{on}, k_{off} and K_d for ATP binding event of F_1-ATPase (Figure 33). From the comparison of kinetic parameters of V_1 and F_1, we could deduce 2 important assertions. One is that ATP-binding site of V_1 has lower affinity to ATP than that of F_1. k_{on} values of V_1 over all stall angles are lower than those of F_1, while k_{off} and K_d are higher.

The second one is that ATP binding does not contribute to torque generation in V_1 as much as it does in F_1 (Figure 33 and 34). Previous study determined the torque contributed by ATP binding in F_1 as 11 pN·nm (21). Here we assume that the torsional rigidity of rotary shaft of V_1 estimated from the rotary potential during pausing state is not so different from that of F_1 (though precise estimation of torsional rigidity of V_1 is required). Based on our experimental data, conformational changes in A subunit induced upon ATP binding are expected to be

smaller as compared to those in β subunit of F_1. For a better understanding of the effect of ATP binding, crystal structures of A subunit with and without bound ATP are awaited.

3.3.2 Implications about ATP synthesis

By using the kinetic parameters determined for ATP binding event, we can also interpret about ATP synthesis. K_d at 0° was 0.7 μM, which is too low to release ATP into cellular medium where ATP concentration is in millimolar range. When we rotate over -162°, then K_d reaches to the millimolar range and V_1 is able to release ATP. In addition, k_{off} at 0° was 0.46 s^{-1} is quite slow to explain the maximum turnover rate of ATP synthesis (67-73 s^{-1}) (36). However, if we rotate the shaft over -277°, then k_{off} could reach the maximum turnover rate. These results suggest that ATP synthesis is not simply the reverse of ATP hydrolysis reaction. Therefore the angular dependence of kinetic and thermodynamic parameters should be considered to have an accurate interpretation of ATP synthesis event. We should not forget that these parameters were most probably overestimated, due to the elasticity of the experimental setup.

3.4 Conclusion

ATP binding event was modulated mechanically using the magnetic tweezers. Strong angle dependency of ATP binding event shows that chemical reactions are modulated by rotation of the shaft. Torque generated by ATP binding event was calculated to be 4 pN·nm, which is quite small compared with the whole torque (35 pN·nm) of V_1 in one single step.

Chapter 4. General Conclusion and Future Work

4.1 General Conclusion

This study was an attempt to shed light on the mechanochemical coupling mechanism of V_1-ATPase by comparison with F_1-ATPase. Even though both V_1- and F_1-ATPases are rotary motor proteins, their subunit arrangements and so far revealed-rotation schemes are different. This study emphasizes their significant differences more, by focusing on the mechanochemical coupling and torque generation mechanism.

We successfully analyzed the ATP binding reaction regarding its angular dependency and kinetic rate constants. We showed that V_1-ATPase displays a strong angular dependency during ATP binding reaction. Moreover, we compared our results with that of F_1 data, which was available from literature. This comparison pointed out that mechanochemical coupling mechanism of V_1 is different from that of F_1 based on the observation that ATP binding reaction is not primary torque-generating step in case of V_1. As a following step for this study, ATP hydrolysis and product release events should be analyzed with mechanical manipulation method to complete the picture of mechanochemical couling mechanism of V_1-ATPase (refer to section **4.2**).

Furthermore, we characterized two pauses of V_1-ATPase which were frequently observed during our manipulation of V_1-ATPase in ATP-binding reaction. We wanted to clarify that these pauses do not interfere with the ATP-binding dwell of V_1-ATPase and we did so. One pause, named as 'short pause', lasted for several seconds. Our analysis wasn't able to reveal its physiological role, however, discovering this pause, itself, was a new finding of this study. Further research is necessary for uncovering the still unknown points about this pause (refer to section **4.3**). We also revealed that the other pause, named as 'long pause',

represents the ADP-inhibited state of V_1-ATPase. Comparison with F_1-ATPase showed that larger activation energy is required for exit from long pause in case of V_1-ATPase.

4.2 Future Work

4.2.1 Mechanical Modulation of ATP hydrolysis

In previous studies, ATP binding, ATP hydrolysis and ADP-inhibited events of F_1 were studied by employing stall-and-release experiment (1,21). As to V_1-ATPase, only ATP binding and long pause (ADP-inhibited state) reactions were studied (38). Based on our results from stall-and-release experiment, ATP binding does not seem to be main torque-generating step in V_1-ATPase. Though, the effect of ATP binding is crucial in case of F_1-ATPase. It was also shown that ATP hydrolysis contributes to whole torque less than ATP binding does.

To our surprise, ATP binding event does not have a role in V_1 as significant as in F_1. To have a general view of torque generation mechanism in ATPase superfamily, further research should be performed on V_1-ATPase. By comparing the rotation mechanism of V_1 with that of F_1, a better understanding on ATPase superfamily could be gained.

4.2.2 Mechanical manipulation of Short Pause State

By performing stall-and-release experiment, we showed that long pause state corresponds to ADP-inhibited state. Yet the physiological role of short pause hasn't been determined. Based on obtained results, we hypothesized that short pause could be an additional suppression mechanism for V_1 to escape from hydrolyzing ATP in case V_1 is detached from the whole complex.

There is a possibility that short pause could be the transition state for lapsing into long pause – ADP-inhibited state. To check this possibility, short pause could be studied using

stall-and-release experiment. V_1 could be stalled for long period of time during short pause, and confirmed whether it will lapse into ADP-inhibited state upon release. By this way, we can expand our knowledge about short pause.

4.2.3 Application Point of View

From the application point of view, this study could inspire ideas for using V_1-ATPase in new technologies, such as blocking the invasion of the cells by viruses and toxins or use V_1-ATPase as a stepping motor to induce a desired biological reaction and so on. Following are some possible ideas for employing V_1-ATPase in applied technologies.

4.2.3.1 Blocking Entry of Viruses and Toxins

Eukaryotic V_oV_1-ATPases are shown to have a role in normal physiology at various intracellular sites and also at a number of disease-related processes, one of which is entry of toxins and viruses. Enveloped viruses such as influenza virus enter cells through acidic endosomal compartments, where low pH triggers pore formation in the membrane. Through these pores viral mRNA or cytotoxic portions of the toxin molecules are translocated into the cytoplasm. pH in endosomes are regulated by the proton pumping V_oV_1-ATPases. Our idea is to engineer eukaryotic V_1-ATPases to have the long pause like their homolog prokaryotic V_1-ATPases. Because pumping by V_o domain is coupled to ATPase activity by V_1 domain, if V_1 domain stops rotation, theoretically V_o will also stop pumping protons. By this way, pH will not be regulated by V_oV_1-ATPase anymore, and the entry of toxin and virus will be inhibited. So, engineering the eukaryotic V_1-ATPases to have a long pause could save the cells from the invasion of viruses and toxins. However, whether

eukaryotic V_1-ATPases have the same 'pause' type of regulation as prokaryotic V_1-ATPases is not clear. So, further single-molecule research on eukaryotic V_1-ATPase is necessary.

4.2.3.2 *Treatment of Osteoporosis*

Osteoporosis is a disease in which bone resorption exceeds bone formation, and results in weakening of the bones. Osteoclasts generate an acidic microenvironment necessary for bone resorption by using V_oV_1-ATPases to pump protons into the resorption area. If V_oV_1-ATPases' pumping protons can be stopped, then osteoporosis could be largely prevented. The way to stop pumping protons could be to prolong short pause state or to induce entering into long pause state. So, engineering V_oV_1-ATPases in this way could be enough for fighting with osteoporosis.

4.2.3.3 *As a stepping motor*

Another application could be to use the V_oV_1-ATPase like a stepping motor, to induce a biological reaction while the V_1-ATPase is rotating and to block the reaction when the motor stopped during short pause. If the reason for short pause is revealed, we could manipulate V_1-ATPase to enter into short pause and resume rotation again at desired time intervals. This type of regulation could reveal insights about the biological reactions.

Appendix Protocols for Experiments

A.1 Purification of Wild Type V_1-ATPase from *E.coli*

Materials

Buffers

Buffer A	100 mM NaPi (pH 8.0), 300 mM NaCl, 20 mM Imidazole (pH 8.0)
Buffer B	100 mM NaPi (pH 8.0), 300 mM NaCl, 200 mM Imidazole-HCl (pH 8.0)
Buffer C	20 mM Tris-HCl (pH 8.0), 1 mM EDTA
Buffer D	20 mM Tris-HCl (pH 8.0), 1 mM EDTA, 1 M NaCl
ADP Removal Buffer	100 mM NaPi (pH 8.0), 10 mM EDTA
Biotinylation Buffer	20 mM MOPS-KOH (pH 7.0), 150 mM NaCl

Filters&Columns

Amicon Ultra Centrifuge Filters (Millipore)

Ni-NTA Column

UNOQ Column (Bio-Rad)

PD-10 gel filtration column

Superdex HR200 GL column (Amersham-Tricorn)

Methods

A.1.1 Preparation of Glycerol Stock of V_1-ATPase Expressing *E.coli*

↓ Transform WT V_1 plasmid (expressing *Thermus thermophilus* V_1-ATPase) into *E.coli BL21 DE3* strain.

↓ Streak the transformed cells into LB plate + Amp + Cam. Incubate overnight.

↓ Pick 8 colonies from the plate, inoculate 4 ml 2xYT medium (+ amp + cam).

↓ Incubate overnight at 37 °C.

↓ Culture

1) Glycerol stock: 600 ul culture + 400 ul from 80 % glycerol stock. Store at -80 °C (either freeze in liquid N_2 or not before storing.)
2) Expression Check: 100 ul culture in 10 ml in 2xYT media (+ Amp

↓ To find the best V_1-ATPase expressing colony, incubate the samples from 2) at 37 °C until O.D. 600 of 0.6 is reached.

↓ Add IPTG (final 1 mM) to induce expression.

↓ Incubate at 37 °C for expression.

↓ Centrifuge the sample at 5000 rpm 10 min at 4 °C.

↓ Discard the supernatant.

↓ Add 1 ml Buffer A, to dissolve the cells.

↓ Sonicate the samples, to break the cell walls of *E.coli.* **total** = 2 or 5 min, **on time** = 1 sec, **off time** = 2 sec

↓ Incubate the broken cell suspension at 65 °C for 30 min, to degrade the thermo-sensitive proteins of *E.coli.*

↓ Centrifuge suspension at 15000 rpm for 10 min.

↓ Analyze the supernatant, by using Native PAGE.

↓ According to expression result, keep only the best expressing colony, discard the others.

A.1.2 Preculture

↓Take 1 or 2 strokes from the V_1 glycerol stock and dissolve it in 15 ml of 2XYT medium (autoclaved) + ampicillin (Diluted 1000x) + chloramphenicol (Diluted 1000x)

↓Shake it in the incubator at 37 °C at max speed

A.1.3 Main Culture

↓Inoculate the mass culture.

↓Shake in the incubator at 37 °C.

↓When O.D. is ≈ 0.6, add IPTG (final conc. 1 mM).

↓Let the cells express V_1-ATPase for about 20 hrs (>16 hrs) at 37 °C.

A.1.4 Harvesting Cells

↓Harvest the cells at 7000 g, 10 min.

↓Discard the supernatant.

↓Dissolve the pellet in ≈100 ml buffer A. Keep the cell suspension on ice.

↓Add one tablet of protease inhibitor cocktail (staying in the 4°C refrigerator). Mix it to dissolve the tablet.

A.1.5 Breaking Cells – Sonication

↓Adjust the tuning of the sonicator to level 4.5.

↓Set the conditions of the sonicator to | total = 5 min, on time = 1 sec, off time = 2 |

A.1.5 Heat Treatment – Degrading Thermo-sensitive Proteins except temperature resistant V_1-ATPase

↓ Keep at 65 °C for 30 min in water bath.

Centrifuge

↓Centrifuge at 10,000 rpm, 90 min at 4 °C.

↓Take the supernatant containing V_1-ATPase, discard the pellet.

A.1.6 Affinity Chromatography

↓Wash with MilliQ twice or 3 times.

↓Equilibrate the column with buffer A.

↓Apply your sample. Let it flow through the column.

↓Wash with buffer A.

↓Elute with buffer B.

↓Check the presence of protein by Bradford Assay.

↓Collect all the fractions where colour change took place.

↓Condense the fractions to 3 ml, by using 50 k amicon centrifugal filter tubes.

↓Exchange the buffer of your sample to buffer C, which is used as wash buffer in AKTA HPLC.

A.1.7 Anion Exchange Chtromatography

↓Wash the pumps with MilliQ.

↓Attach the column.

↓Wash the column with MilliQ.

↓Equilibrate the column and also the pumps with buffer C.

↓Attach the sample loop.

↓Apply your sample.

↓Run the program, collect the fractions containing V_1-ATPase.

↓Condense the fractions to multiples of 2.5 ml by using amicon centrifugal filters.

A.1.8 Removal of Bound ADP

↓Repeat ADP removal protocol (below) for ≈5 times

(reaching ATPase activity of 50 s^{-1} would be enough).

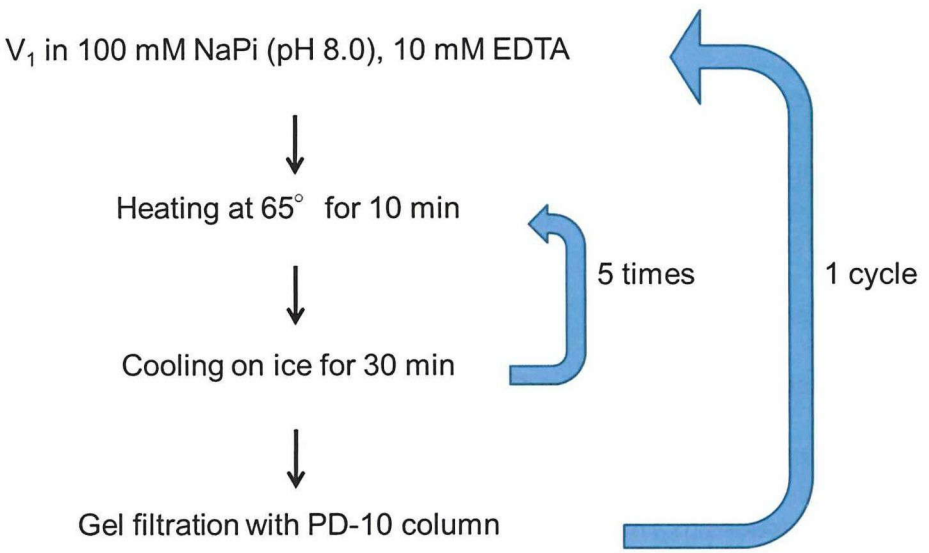

A.1.9 Reducing Disulfide Bonds with DTT

↓Incubate sample with DTT (final conc. 1 mM) at room temp for ≈2 hrs.

↓Condense sample to 500 ul.

A.1.10 Gel Filtration Chromatography

↓Do the washing with MilliQ and equilibration with biotinylation buffer.

↓Inject your sample, collect fractions.

A.1.11 Biotinylation

↓Incubate sample with maleimide-PEG_2-biotin in ratio of $[V_1]$: [Biotin] = 1 : 5

↓Incubate at room temp for 2-3 hrs.

↓Remove excess biotin using PD-10 column.

↓Make aliquots. Freeze in liquid N_2. Store in -80 °C.

A.2 ATPase Activity Measurement

By using ATP regeneration system, ATPase activity of V_1-ATPase is measured (44). This system allows us to measure ATPase activity at constant [ATP]. Absorbance at 340 nm is monitored by UV/VIS spectrophotometer (VP-550, Jasco), as a measure of ATP hydrolysis rate. As seen in the reaction scheme below (Fig. 35), synthesis of 1 ATP molecule results in oxidation of 1 NADH molecule.

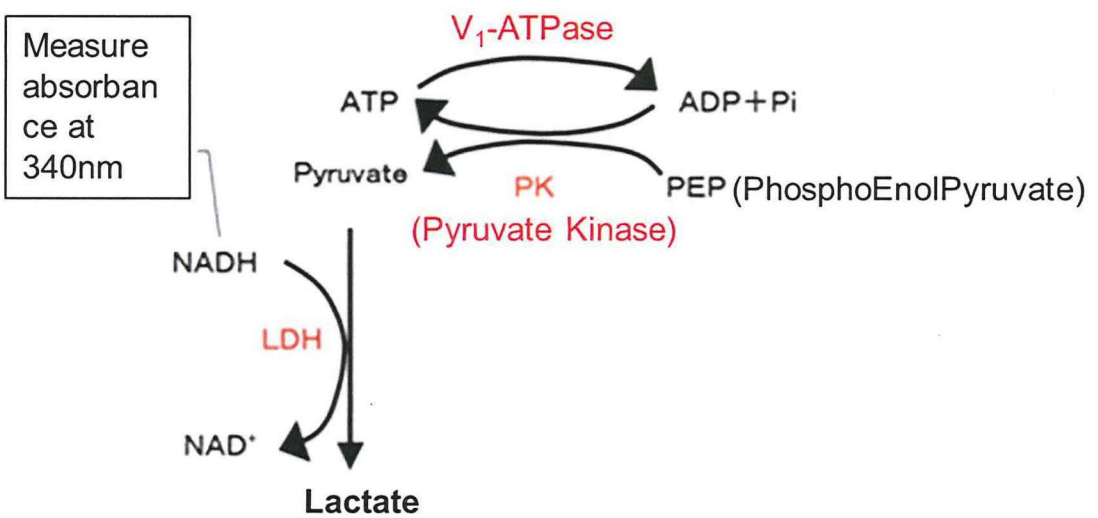

Figure 35. V_1-ATPase activity measurement by decay in NADH oxidation.

$$\text{ATPase(turnover/s)} = \frac{\text{slope(dAbs/min)}}{60 \times 6220^* \times [V_1(M)]}$$

*NADH molar extinction coefficient at 340nm

A.3 Rotation Assay

A.3.1 Preparation of Ni-NTA-Glass

Materials

Glass coverslips (24 x 32 mm)

Glass holder

3-mercaptopropyltrimethoxysilane(MPTMS)

Maleimido-C3-NTA (Dojindo)

DTT, Chloroform, Toluene, Ethanol

Methods

Cleaning the Surface of the Coverslips

- Put the 24 x 32 mm glasses into glass holder, and soak it into ethanol (99.5 %).

  Bath sonicate for 15 min, to remove dust from the glass surface.

Forming Hydroxyl Groups on the Glass Surface (O_2 Etching)

- Dry the glasses with nitrogen gas.
- Locate the glass holder into reactive ion etcher.
- Perform O_2 plasma treatment for 5 mins.

Silanization (Using organic solvents)

- Incubate the glass holder for 1 hr in toluene + MPTMS solution, in ratio of toluene : MPTMS = 100 : 1, with constant stirring.
- Wash with chloroform, ethanol and MilliQ, in order.
- Soak in DTT solution (100 mM Tris-HCl, 1 mM EDTA, 10 mM DTT) for 3 hours.
- Wash in MilliQ.
- Incubate glasses with maleimido-C3-NTA solution (5 mg dissolved in 600 ul pH 7.0 solution) at RT.
- Wash in MilliQ.
- Store in MilliQ at 4 °C.

Incubation with Ni^{2+} solution

- Just before using the glass for rotation assay, incubate the glass with solution ≈50 mM $NiSO_4$ for >5 mins.
- Wash with MilliQ again, dry with air blower.

A.3.2 Magnetic Bead Preparation

Materials

Streptavidin coated magnetic beads, average diameter of ≈500 nm (Seradym seramag)

Method

1) Take 30 ul from the bead stock.
2) Sonication(just very short: 5 sec-10 sec)
3) Dilute beads in 1 ml of MilliQ.
4) Centrifuge at 3000 rpm, 2 min at 4 °C.

5) Take supernatant, discard pellet.

6) Centrifuge at 15k rpm, 60-90 sec at 4 °C.

7) Ppt. (Discard the sup.)

Repeat if needed.

8) Add 200 µl of 0.5x Buffer(-ATP buffer).

9) Add 50-70 µl of 0.5x Buffer(respectively for 30-50 µl)

10) Store at 4 °, until usage.

11) Before usage, pipette, and sonicate for very short; and then rotate in table-top centrifuge for very short (20 - 30 secs).

A.3.3 Rotation Assay

Materials

Ni-NTA glass

Parafilm

Grease

Coverslip(18 x 18 mm)

BSA

-ATP buffer (0.5x Buffer)	+ATP Buffer
• 25 mM Tris-HCl pH 8.0 • 50 mM KCl	• 50 mM Tris-HCl pH 8.0 • 100 mM KCl } 1x Buffer • 2 mM $MgCl_2$ • PEP, PK • ATP-Mg (0.5µM - non-saturating [ATP] ≈ 4 mM - Saturating [ATP])

Method

1) Cut from parafilm in 2.5 x 25 mm size. Expose it in grease. Then place these parafilms on the glass, making sections having size of ≈(3-5) x 25 mm size.
2) Put a coverslip (18 mm x 18 mm) on top of Ni-NTA glass. Press it so that coverslip, greased parafilms and Ni-NTA glasses will be sticked to each other, tightly.
3) Sample was diluted in –ATP buffer (final conc. 1 nM to 4 nM).
4) Infuse V_1-ATPase into the chamber → 5'
5) Wash once with 45 µl –ATP buffer.
6) Infuse 20 µl (- ATP buffer + BSA(5-10 mg/ml)) buffer.
7) (Sonicate the beads for 1 sec.) Beads directly apply 5 µl into the chamber (20' to 30').
8) Move to the microscope stage towards the end of the bead incubation time. Check the beads.
9) Wash with –ATP buffer (70 µl).
10) Infuse ≈ 140 µl of +ATP buffer.
11) Observe rotation.

A.4 Mechanical Manipulation with Magnetic Tweezers

↓ A magnetic tweezers composed of 2 pairs of electromagnets were attached to the microscope stage, as seen in Fig. 36.

↓ Tweezers is controlled with a custom-made software.

↓ For example, during the pause at binding angle, i.e. when the molecule is waiting for ATP to bind, the tweezers is turned on to stall the molecule at a certain angle for a certain period of time.

*Under the condition that ATP binding is the rate-limiting step, 3-step rotation of V_1-ATPase can be observed. Pauses at each step correspond to dwell time for one A subunit from A_3B_3 ring of V_1-ATPase to bind ATP.

↓ After certain time period lapsed; the tweezers is turned off to release the molecule from the magnetic field.

↓Before, during and after this stalling, the molecule's rotation is recorded at 30 fps.

↓The behavior of the molecule upon release from the magnetic field is analyzed by image analysis software, Digimo.

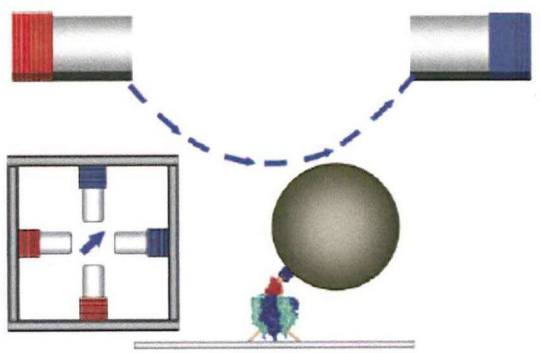

Figure 36. Magnetic Tweezers and Manipulation of the Bead by applied Magnetic Field (1)

A.4.1 Analysis of the Manipulation Data

↓ Mainly two behaviors were observed, as summarized in Fig. 37.

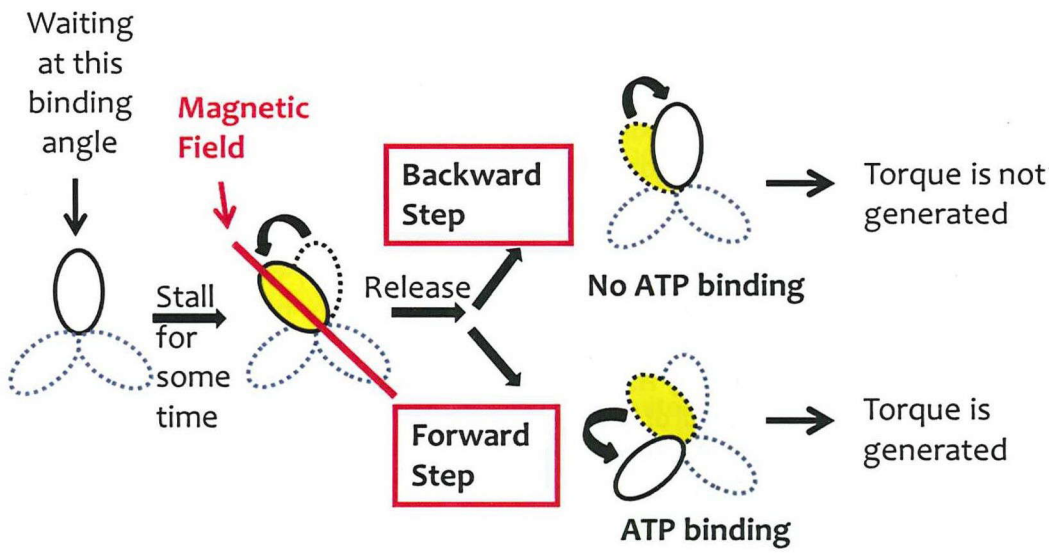

Figure 37. Forward and backward step upon release from the tweezers

- Forward step: Upon release from the tweezers, therefore from the magnetic field, molecule goes to next binding angle, implying that molecule **was** bound ATP when it was released from tweezers.

- Backward step: Upon release from the magnetic field, molecule goes back to original binding angle, implying that molecule **was not** bound ATP when it was released from tweezers.

↓ Probability of occurrence of forward step is calculated as a measure of effect of mechanical manipulation on ATP binding event. Using KaleidaGraph graphing software, graphs of forward step probability (FSP) vs stalling angle or stalling time is drawn.

$$\text{ForwardStep Probability (FSP)} = \frac{\text{ForwardStep}}{\text{ForwardStep} + \text{BackwardStep}}$$

REFERENCES

1. Hirono-Hara, Y., Ishizuka, K., Kinosita, K., Jr., Yoshida, M., and Noji, H. (2005) Activation of pausing F1 motor by external force. *Proceedings of the National Academy of Sciences of the United States of America* **102**, 4288-4293
2. Forgac, M. (2007) Vacuolar ATPases: rotary proton pumps in physiology and pathophysiology. *Nature reviews. Molecular cell biology* **8**, 917-929
3. Nishi, T., and Forgac, M. (2002) The vacuolar (H+)-ATPases--nature's most versatile proton pumps. *Nature reviews. Molecular cell biology* **3**, 94-103
4. Yokoyama, K., and Imamura, H. (2005) Rotation, structure, and classification of prokaryotic V-ATPase. *Journal of bioenergetics and biomembranes* **37**, 405-410
5. Yokoyama, K., Muneyuki, E., Amano, T., Mizutani, S., Yoshida, M., Ishida, M., and Ohkuma, S. (1998) V-ATPase of Thermus thermophilus is inactivated during ATP hydrolysis but can synthesize ATP. *The Journal of biological chemistry* **273**, 20504-20510
6. Yokoyama, K., Oshima, T., and Yoshida, M. (1990) Thermus thermophilus membrane-associated ATPase. Indication of a eubacterial V-type ATPase. *The Journal of biological chemistry* **265**, 21946-21950
7. Iwata, M., Imamura, H., Stambouli, E., Ikeda, C., Tamakoshi, M., Nagata, K., Makyio, H., Hankamer, B., Barber, J., Yoshida, M., Yokoyama, K., and Iwata, S. (2004) Crystal structure of a central stalk subunit C and reversible association/dissociation of vacuole-type ATPase. *Proceedings of the National Academy of Sciences of the United States of America* **101**, 59-64
8. Yokoyama, K., Nagata, K., Imamura, H., Ohkuma, S., Yoshida, M., and Tamakoshi, M. (2003) Subunit arrangement in V-ATPase from Thermus thermophilus. *The Journal of biological chemistry* **278**, 42686-42691
9. Yoshida, M., Muneyuki, E., and Hisabori, T. (2001) ATP synthase--a marvellous rotary engine of the cell. *Nature reviews. Molecular cell biology* **2**, 669-677
10. Diez, M., Zimmermann, B., Borsch, M., Konig, M., Schweinberger, E., Steigmiller, S., Reuter, R., Felekyan, S., Kudryavtsev, V., Seidel, C. A., and Graber, P. (2004) Proton-powered subunit rotation in single membrane-bound FoF1-ATP synthase. *Nature structural & molecular biology* **11**, 135-141
11. Kato, Y., Matsui, T., Tanaka, N., Muneyuki, E., Hisabori, T., and Yoshida, M. (1997) Thermophilic F1-ATPase is activated without dissociation of an endogenous inhibitor, epsilon subunit. *The Journal of biological chemistry* **272**, 24906-24912
12. Jiang, W., Hermolin, J., and Fillingame, R. H. (2001) The preferred stoichiometry of c subunits in the rotary motor sector of Escherichia coli ATP synthase is 10. *Proceedings of the National Academy of Sciences of the United States of America* **98**, 4966-4971
13. Mitome, N., Suzuki, T., Hayashi, S., and Yoshida, M. (2004) Thermophilic ATP synthase has a decamer c-ring: indication of noninteger 10:3 H+/ATP ratio and permissive elastic coupling. *Proceedings of the National Academy of Sciences of the United States of America* **101**, 12159-12164
14. Imamura, H., Nakano, M., Noji, H., Muneyuki, E., Ohkuma, S., Yoshida, M., and Yokoyama, K. (2003) Evidence for rotation of V1-ATPase. *Proceedings of the National Academy of Sciences of the United States of America* **100**, 2312-2315

15. Imamura, H., Takeda, M., Funamoto, S., Shimabukuro, K., Yoshida, M., and Yokoyama, K. (2005) Rotation scheme of V1-motor is different from that of F1-motor. *Proceedings of the National Academy of Sciences of the United States of America* **102**, 17929-17933
16. Kinosita, K., Jr., Adachi, K., and Itoh, H. (2004) Rotation of F1-ATPase: how an ATP-driven molecular machine may work. *Annual review of biophysics and biomolecular structure* **33**, 245-268
17. Furuike, S., Nakano, M., Adachi, K., Noji, H., Kinosita, K., Jr., and Yokoyama, K. (2011) Resolving stepping rotation in Thermus thermophilus H(+)-ATPase/synthase with an essentially drag-free probe. *Nature communications* **2**, 233
18. Abrahams, J. P., Leslie, A. G., Lutter, R., and Walker, J. E. (1994) Structure at 2.8 A resolution of F1-ATPase from bovine heart mitochondria. *Nature* **370**, 621-628
19. Boyer, P. D. (1997) The ATP synthase--a splendid molecular machine. *Annual review of biochemistry* **66**, 717-749
20. Noji, H., Yasuda, R., Yoshida, M., and Kinosita, K., Jr. (1997) Direct observation of the rotation of F1-ATPase. *Nature* **386**, 299-302
21. Watanabe, R., Okuno, D., Sakakihara, S., Shimabukuro, K., Iino, R., Yoshida, M., and Noji, H. (2012) Mechanical modulation of catalytic power on F1-ATPase. *Nature chemical biology* **8**, 86-92
22. Yasuda, R., Noji, H., Kinosita, K., Jr., and Yoshida, M. (1998) F1-ATPase is a highly efficient molecular motor that rotates with discrete 120 degree steps. *Cell* **93**, 1117-1124
23. Shimabukuro, K., Yasuda, R., Muneyuki, E., Hara, K. Y., Kinosita, K., Jr., and Yoshida, M. (2003) Catalysis and rotation of F1 motor: cleavage of ATP at the catalytic site occurs in 1 ms before 40 degree substep rotation. *Proceedings of the National Academy of Sciences of the United States of America* **100**, 14731-14736
24. Yasuda, R., Noji, H., Yoshida, M., Kinosita, K., Jr., and Itoh, H. (2001) Resolution of distinct rotational substeps by submillisecond kinetic analysis of F1-ATPase. *Nature* **410**, 898-904
25. Adachi, K., Oiwa, K., Nishizaka, T., Furuike, S., Noji, H., Itoh, H., Yoshida, M., and Kinosita, K., Jr. (2007) Coupling of rotation and catalysis in F(1)-ATPase revealed by single-molecule imaging and manipulation. *Cell* **130**, 309-321
26. Ariga, T. (2008) The concerted nature between three catalytic subunits driving the F1 rotary motor. *Bio Systems* **93**, 68-77
27. Enoki, S., Watanabe, R., Iino, R., and Noji, H. (2009) Single-molecule study on the temperature-sensitive reaction of F1-ATPase with a hybrid F1 carrying a single beta(E190D). *The Journal of biological chemistry* **284**, 23169-23176
28. Watanabe, R., Iino, R., and Noji, H. (2010) Phosphate release in F1-ATPase catalytic cycle follows ADP release. *Nature chemical biology* **6**, 814-820
29. Watanabe, R., Iino, R., Shimabukuro, K., Yoshida, M., and Noji, H. (2008) Temperature-sensitive reaction intermediate of F1-ATPase. *EMBO reports* **9**, 84-90
30. Hirono-Hara, Y., Noji, H., Nishiura, M., Muneyuki, E., Hara, K. Y., Yasuda, R., Kinosita, K., Jr., and Yoshida, M. (2001) Pause and rotation of F(1)-ATPase during catalysis. *Proceedings of the National Academy of Sciences of the United States of America* **98**, 13649-13654
31. Jault, J. M., and Allison, W. S. (1994) Hysteretic inhibition of the bovine heart mitochondrial F1-ATPase is due to saturation of noncatalytic sites with ADP which

blocks activation of the enzyme by ATP. *The Journal of biological chemistry* **269,** 319-325

32. Kakinuma, Y., Yamato, I., and Murata, T. (1999) Structure and function of vacuolar Na+-translocating ATPase in Enterococcus hirae. *Journal of bioenergetics and biomembranes* **31,** 7-14
33. Iko, Y., Tabata, K. V., Sakakihara, S., Nakashima, T., and Noji, H. (2009) Acceleration of the ATP-binding rate of F1-ATPase by forcible forward rotation. *FEBS letters* **583,** 3187-3191
34. Yokoyama, K., Akabane, Y., Ishii, N., and Yoshida, M. (1994) Isolation of prokaryotic V0V1-ATPase from a thermophilic eubacterium Thermus thermophilus. *The Journal of biological chemistry* **269,** 12248-12253
35. Imamura, H., Ikeda, C., Yoshida, M., and Yokoyama, K. (2004) The F subunit of Thermus thermophilus V1-ATPase promotes ATPase activity but is not necessary for rotation. *The Journal of biological chemistry* **279,** 18085-18090
36. Nakano, M., Imamura, H., Toei, M., Tamakoshi, M., Yoshida, M., and Yokoyama, K. (2008) ATP hydrolysis and synthesis of a rotary motor V-ATPase from Thermus thermophilus. *The Journal of biological chemistry* **283,** 20789-20796
37. Yokoyama, K., Nakano, M., Imamura, H., Yoshida, M., and Tamakoshi, M. (2003) Rotation of the proteolipid ring in the V-ATPase. *The Journal of biological chemistry* **278,** 24255-24258
38. Uner, N. E., Nishikawa, Y., Okuno, D., Nakano, M., Yokoyama, K., and Noji, H. (2012) Single-molecule Analysis of Inhibitory Pausing States of V1-ATPase. *The Journal of biological chemistry* **287,** 28327-28335
39. Okuno, D., Fujisawa, R., Iino, R., Hirono-Hara, Y., Imamura, H., and Noji, H. (2008) Correlation between the conformational states of F1-ATPase as determined from its crystal structure and single-molecule rotation. *Proceedings of the National Academy of Sciences of the United States of America* **105,** 20722-20727
40. Cherepanov, D. A., and Junge, W. (2001) Viscoelastic dynamics of actin filaments coupled to rotary F-ATPase: curvature as an indicator of the torque. *Biophysical journal* **81,** 1234-1244
41. Sielaff, H., Rennekamp, H., Wachter, A., Xie, H., Hilbers, F., Feldbauer, K., Dunn, S. D., Engelbrecht, S., and Junge, W. (2008) Domain compliance and elastic power transmission in rotary F(O)F(1)-ATPase. *Proceedings of the National Academy of Sciences of the United States of America* **105,** 17760-17765
42. Takeda, M., Suno-Ikeda, C., Shimabukuro, K., Yoshida, M., and Yokoyama, K. (2009) Mechanism of inhibition of the V-type molecular motor by tributyltin chloride. *Biophysical journal* **96,** 1210-1217
43. Makyio, H., Iino, R., Ikeda, C., Imamura, H., Tamakoshi, M., Iwata, M., Stock, D., Bernal, R. A., Carpenter, E. P., Yoshida, M., Yokoyama, K., and Iwata, S. (2005) Structure of a central stalk subunit F of prokaryotic V-type ATPase/synthase from Thermus thermophilus. *The EMBO journal* **24,** 3974-3983
44. Schweins, T., and Warshel, A. (1996) Mechanistic analysis of the observed linear free energy relationships in p21ras and related systems. *Biochemistry* **35,** 14232-14243

PUBLICATIONS

1. **Uner, N. E.**, Nishikawa, Y., Okuno, D., Nakano, M., Yokoyama, K., and Noji, H. (2012) Single-molecule Analysis of Inhibitory Pausing States of V_1-ATPase. *The Journal of Biological Chemistry* **287**, 28327-28335

2. **Tirtom, N.E.**, Okuno, D., Nakano, M., Yokoyama, K., and Noji, H. (2012) Mechanical Modulation of ATP-Binding Affinity of V_1-ATPase – *Submitted*

ACKNOWLEDGMENTS

This thesis marks the end of my path in obtaining PhD degree. Up to this point, I collected a lot of memorable moments in Noji laboratory, Osaka university and lastly in the University of Tokyo. This thesis would not have been completed without the support and encouragement of numerous people, to only some of whom particular mention is given here.

First of all, I would like to express my deep gratitude and heartfelt thanks to my advisor, Prof. Hiroyuki Noji. Under his guidance, I felt more enthusiastic about doing research. His help of constructive comments and suggestions throughout the experimental work have contributed to the success of this research. His friendliness and understanding, especially, throughout this year means a lot to me, because I was not able to use my right hand efficiently due to injury.

I also would like to thank my supervisor Prof. Masahiro Kino-oka, for helpful discussions and encouragement.

I am also greatly indebted to my senior advisor, Dr. Daichi Okuno for his support and patience in teaching me. I learned a lot about how to do research professionally from watching him.

I would like to express my sincere appreciation to Dr. Masahiro Nakano, for teaching me the details of purification and rotation assay of V_1-ATPase. He has not only been a good mentor, but also a good friend to me. His working discipline is one of his features I would like to inherit from him.

I also would like to express my thanks to Yoshihiro Nishikawa for starting the research about 'pauses of V_1-ATPase'.

I would like to thank Prof. Ken Yokoyama for his invaluable comments and discussions during the experimental and paper work.

I would like to express my appreciation to each of my current and former labmates in Noji Laboratory for the valuable discussions and all the fun we've had together in last five years. I should thank Dr. Rikiya Watanabe for critical discussions and valuable comments, Dr. Hiromi Imamura for his invaluable advices and triggering enthusiasm for my own project, Dr. Kumiko Hayashi for all of the teachings about Jonathan Howard's book on motor proteins and pushing me to participate more actively to scientific discussions, Ms. Huijuan You for guidance during all these years and studying the principles of motor proteins with me, Dr. Masashi Toei for guidance about my PhD defense presentation, Dr. Mizue Tanigawara for help about the experimental work.

I would like to acknowledge secretaries of Noji Laboratory, Ms. Sakai and Ohta, for all the help they rendered me during my stay in Japan.

I would like to thank Osaka University and Japanese Government for giving me this oppurtunity to do research with financial support.

My special thanks goes to my husband, Dr. Ismail Tirtom. Last two years have been much easier for me because of his continuous help and guidance. With him, I feel more courageous.

At this juncture, my deepest gratitude goes to my beloved parents and brothers: Suheyla, Ali Suat, Emir and Mahmut Celalettin Uner. Without their encouragement and support, I

could not have been brave enough to study in abroad in the first place. The success of this research has been possible due to their selfless sacrificies. Therefore I dedicate this work to my parents and brothers.

Finally, I would like to thank all those people who directly or indirectly have contributed to completion of this thesis.